UNIVERSITY OF CALIFORNIA, MERCED

Investigation of the Interaction between the CC-chemokine Eotaxin and the Viral CC-Chemokine Inhibitor vCCI

A Thesis submitted in partial satisfaction of the requirements
for the degree Master of Science

in

Quantitative and Systems Biology

By

Wei Tian

2009

UNIVERSITY OF CALIFORNIA, MERCED

Investigation of the Interaction between the CC-chemokine Eotaxin and the Viral CC-Chemokine Inhibitor vCCI

A Thesis submitted in partial satisfaction of the requirements
for the degree Master of Science

in

Quantitative and Systems Biology

By

Wei Tian

Committee in charge:

Professor Patricia J. LiWang, Principal Investigator

Professor Andy LiWang, Chair

Professor David M Ojcius

Professor Jinah Choi

2009

The Thesis of Your Full Legal Name is approved and it is acceptable in quality and form for publication on microfilm and electronically:

_____

_____

_____

_____

Chair

University of California, Merced

2009

DEDICATION

I dedicate this work to my dear parents and sisters for their unconditional love. It's your encouragement and consistent trust of my capability that help me to come so far.

I also give my gratitude to my primary advisor, Dr. Patricia J. LiWang. Her sensible guidance and thoughtful advice are critical for finishing this work.

TABLE OF CONTENTS

Signature Page……..……..... iii

Dedication iv

Table of Contents..... v

List of Figures..... vi

List of Tables..... viii

Acknowledgements ix

Abstract……. x

Chapter 1 Introduction
1.1 Immune System…….....……..... 1
1.2 Chemokines and their receptors…….…….... 1
1.3 Viral CC chemokine inhibitors 8

Chapter 2 Investigation of the Essential Binding Residues of Eotaxin Through Mutagenesis and Fluorescence Anisotropy…….... 14
2.1 Introduction 14
2.1 Materials and methods 19
2.3 Results 25

Chapter 3 Investigation of the Essential Binding Residues of vCCI Through Mutagenesis and Fluorescence Anisotropy
3.1 Introduction 42
3.2 Materials and methods 44
3.3 Results 47

Chapter 4 Making Crystals of the Complex Composed of Eotaxin and vCCI
4.1 Introduction 57
4.2 Materials and methods 57
4.3 Results 58

Chapter 5 Summary and Conclusion..... 64

Supplemental Material …….. 66

References..... 68

LIST OF FIGURES

Figure 1.1: Ribbon diagram of common chemokine structure represented by eotaxin…… 4

Figure 1.2: Overview of how an antigen initiates the chemotaxis of leukocytes… 5

Figure 1.3: Diagram of vCCI structure of compox virus …… 10

Figure 1.4: Binding mechanism between vCCI and MIP-1β…….....…… 12

Figure 2.1: Sequence alignment of the human CC chemokines with high affinity towards vCCI…….. 16

Figure 2.2: The vCCI-binding determinants of MCP-1 ……..... 17

Figure 2.3: The mechanism of fluorescence anisotropy ……. 18

Figure 2.4.1: The 2nd-step purification HPLC spectrum of eotaxin-C75-fluo eluted from G25 size exclusion column ……..…..... 24

Figure 2.4.2: Coomassie staining image of SDS-PAGE of the products eluted from size column and from C4 column …… 24

Figure 2.4.3: UV-image of SDS-PAGE of the products eluted from size column and from C4 column ……... 24

Figure 2.5: Interactions between eotaxin and vCCI shown by NMR spectrum …. 26

Figure 2.6.1: Overlay of wild type eotaxin (black) and eotaxin-C75 (red)…… 27

Figure 2.6.2: Overlay of wild type eotaxin (black) and fluorophore-labeled eotaxin-C75 (red) ……...……. 27

Figure 2.7.1: Overlay of wild type eotaxin (black) and F11A eotaxin (red)…….... 29

Figure 2.7.2: Overlay of wild type eotaxin (black) and R16A eotaxin (red). The peak of R16 is gone in R16A eotaxin …….……. 29

Figure 2.7.3: Overlay of wild type eotaxin (black) and R22E eotaxin (red). The peak of R22 is gone in R22E eotaxin ……..…… 30

Figure 2.7.4: Overlay of wild type eotaxin (black) and K44A eotaxin (red). The peak of K44 is gone in K44A eotaxin ……. 30

Figure 2.7.5: Overlay of wild type eotaxin (black) and K47A eotaxin (red). The peak of K47 is gone in K44A eotaxin …… 31

Figure 2.7.6: Overlay of wild type eotaxin (black) and R16AR22E eotaxin (red). The peaks of R16 and R22 are gone in R16AR22E eotaxin ……. 31

Figure 2.7.7: Overlay of wild type eotaxin (black) and R22AK44A eotaxin (red). The peaks of R22 and K44 are gone in R22AK44A eotaxin …… 32

Figure 2.7.8: Overlay of wild type eotaxin (black) and R22EK44A eotaxin (red). The peaks of R22 and K44 are gone in R22EK44A eotaxin ……. 32

Figure 2.8: Titration of eotaxin-fluo with vCCI monitored by fluorescence anisotropy …….. 34

Figure 2.9: Competition binding curve for eotaxin mutants against eot-fluo …… 36

Figure 2.10: Relative binding difference between wild type eotaxin and mutants based on K_d values ……. 37

Figure 2.11: Relative binding difference between wild type eotaxin and mutants based on IC_{50} values …… 39

Figure 3.1: Sequence alignment of three members of the orthopox vCCI family showing high homology along with another virus protein VACV A41 sharing low homology ……. 43

Figure 3.2: Overlay of ^{15}N HSQC of unbound vCCI (black) and complex vCCI:eotaxin (red) …….. 48

Figure 3.3: Overlay of ^{15}N HSQC of wild type vCCI (black) and D141K vCCI (red)…….. 49

Figure 3.4: Titration of eotaxin-fluo with D141A vCCI monitored by fluorescence anisotropy ……..**.....** 51

Figure 4.1.1: Elution spectrum of the complex of eotaxin:vCCI using G75 size exclusion column ……...……..**.....** 59

Figure 4.1.2: Commassie blue staining image of the SDS-PAGE of the fractions eluted from G75 size column ……..... 59

Figure 4.3: Crystals with needle-like shape were observed by optical microscope with 100 fold amplification ……..…… 60

Figure 4.4: Crystals observed by optical microscope with 100 fold amplification. 61

LIST OF TABLES

2.1 Binding affinity constants (K_d) of eotaxin variants ……..... 35

2.2 Half maximal inhibitory concentration values (IC50) of eotaxin variants .. 38

3.1 Proteins and/or plasmids of mutants used or made made in this project…. 46

3.2 Binding affinity constants (K_d) of eotaxin variants ……. 52

ACKNOWLEDZGEMENTS

I would like to thank my committee members, Drs. Andy LiWang, David Ojcius, Jinah Choi, for their advice for this project.

Millions of thanks also go to my friends and colleagues who accompanied me during this journey of study.

Funding for this work was provided by National Institution of Health Grants AI47832 and AI070993.

ABSTRACT OF THE THESIS

Investigation of the Interaction Mechanism between CC-chemokine Eotaxin and Virus CC-Chemokine Inhibitor vCCI

by

Wei Tian

Master of Science

University of California, Merced, 2009

Professor Andy LiWang, Chair

Eotaxin belongs to the chemokine family of proteins, which are involved in inflammation and in the development of the immune system, regulating activation and chemotaxis of leukocytes. Chemokines are involved in a variety of inflammatory diseases such as rheumatoid arthritis and allergic asthma. The viral protein CC-chemokine inhibitor (vCCI) from poxviruses can bind many different chemokines with

high affinity, which makes it a potentially valuable therapeutic agent to treat such inflammatory diseases. However, it is not clear how vCCI is able to bind so many different chemokines. NMR data from the vCCI:MIP-1β complex and preliminary vCCI:eotaxin NMR data indicates that in eotaxin Phe11, Arg16, Arg 22, Lys 44, and possibly Lys 47 are involved in binding vCCI. Correspondingly, Tyr217, Phe215, Val185, along with Asp141, Glu143 and a flexible acidic loop in vCCI are involved in binding eotaxin. Mutations were made in these residues and binding to vCCI was tested by fluorescence anisotropy. This project investigates the interaction of chemokines and vCCI at a molecular level through NMR, mutagenesis, and fluorescence anisotropy studies.

The results of investigation show that residues Phe11, Arg16, Arg 22, Lys 44 in eotaxin are involved in binding vCCI. Single mutations in Asp141, Glu143 of vCCI do not show significant change in binding affinity. More mutations such as a double mutant D141A/E143A vCCI, mutants of other nearby acidic residues (e.g. Asp73, Asp75), need to be done before any conclusion is made.

Chapter 1

Introduction

1.1 Immune System

The immune system is defined as a biological network of coordinated pathways within an organism which protects against pathogens and tumors. There are two responding mechanisms coordinated in immune protection: innate and adaptive immunity. Innate immunity provides the early lines of defense against all pathogens in which leukocytes are recruited to the site of infection and activated to eliminate the infection. It consists of the following components: (1) epithelial barriers and anti-pathogen substances, such as antibiotic peptides and some cytokines secreted at the epithelial surfaces; (2) phagocytic cells (such as neutrophils and macrophages), natural killer cells, etc.; (3) the complement system composed of several plasma proteins that induce phagocytosis of the pathogens; (4) cytokines such as CC chemokines that are used to recruit and activate leukocytes, to enhance the synthesis of effector cells and proteins for the anti-pathogen responses. If pathogens get past innate immunity, they confront the body's adaptive immunity, which is specific for distinct macromolecules of individual pathogen and is able to remember and respond more vigorously to repeated exposures to the same pathogens. Adaptive immunity is a highly evolved defense response; it is composed of lymphocytes (like T cell, B cells, natural killer cells) and their products (antibodies, cytotoxic granules, cytokines, etc.). (1)

1.2 Chemokines and their receptors

In the immune system, chemokines are produced and used as signaling messengers to guide the migration of nearby responsive cells, particularly to regulate the activation and chemotaxis of leukocytes. There are two types of chemokines based on their function: inflammatory and homeostatic. Homeostatic chemokines are constitutively expressed in restricted tissue(s), and responsible for regulating lymphocyte migration and the compartmentalization of lymphoid organs. This group includes SLC, ELC, SDF-1. Typical inflammatory chemokines include eotaxin, MCP-1, MIP-1β and RANTES, which are released from a wide variety of cells including endothelial cells, in response to pathogens and agents such as silica that cause physical damages. Inflammatory chemokines recruit cells from both innate and adaptive immune systems such as eosinophils, basophils and monocytes from the bloodstream to infected or damaged sites and stimulate inflammatory reactions (2, 3, 4).

In general, chemokines (chemotactic cytokines**)** are a family of small cytokines (*cyto*-, cell; and *-kinos*, movement), with MW ranging from 8 to 14 kDa. After the first chemokine, IL-8, was discovered in 1987 (5), about 50 additional chemokines have been identified to date (6). These chemokines are divided into 4 subfamilies based on the arrangement of the two N-terminal cysteines. The CC subfamily (in which the two cysteines are adjacent) and the CXC subfamily (in which the two cysteines are separated by one non-conserved amino acid) are the two major groups; CX3C and C subfamilies are the two minor subfamilies. The CC chemokine consists of at least 27 proteins including EOTAXIN, MCP-1 and MIP-1β. CC chemokines regulate the migration of

leukocytes such as eosinophils and monocytes, along with other cell types such as NK cells and dendritic cells. The CXC chemokine family is composed of about 17 members including IL-8 and BCA-1; they are involved in the recruitment of lymphocytes and leukocytes like neutrophils. The C chemokine family has two members: XCL1 and XCL2. The CX_3C chemokine family has one member, fractalkine. Chemokines share 25-50% identity, and have several conserved cysteine residues that interact with each other to form a disulfide bond to establish their unique 3-dimensional structure. Structures of different chemokines such as eotaxin and MIP-1β have been investigated with the techniques of NMR and/or X-ray crystallography, which show a common conformation of a Greek key shape (7,8). This common structure is represented by monomeric eotaxin in Figure 1.1. This chemokine's structure starts with an unstructured N-terminus and a long flexible loop known as N-loop, followed by a single-turn helix, three antiparallel β-strands and a C-terminal α-helix. As for the function of different parts of chemokines, generally the N-loop region is used to bind with the receptor, while the unstructured N-terminus is involved in receptor activation, and a 40's loop and C-terminal helical region are used in GAG (Glycosaminoglycans) binding (9-12).

The major function of chemokines is to direct the migration of immune cells as a chemoattractant; responding cells follow an increasing chemokine gradient towards the target sites. This process, called chemotaxis, is shown in Figure 1.2. The most popular model of the chemotaxis is as follows: After being secreted from tissue cells such as epithelial cells, chemokines bind to the GAGs presented on the epithelial surface with low affinity. Chemokines are in a dynamic equilibrium process between dimers (or

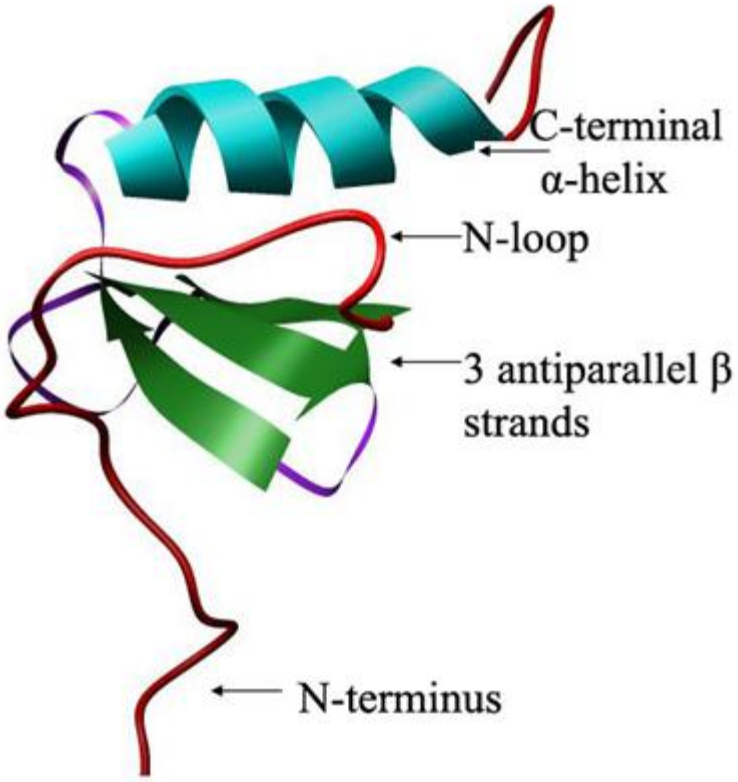

Figure 1.1. Ribbon diagram of common chemokine structure represented by eotaxin. This tertiary conformation starts with an extended N-ternimus and an N-loop, followed by three anti-parallel β strands and a C-terminal α-helix.

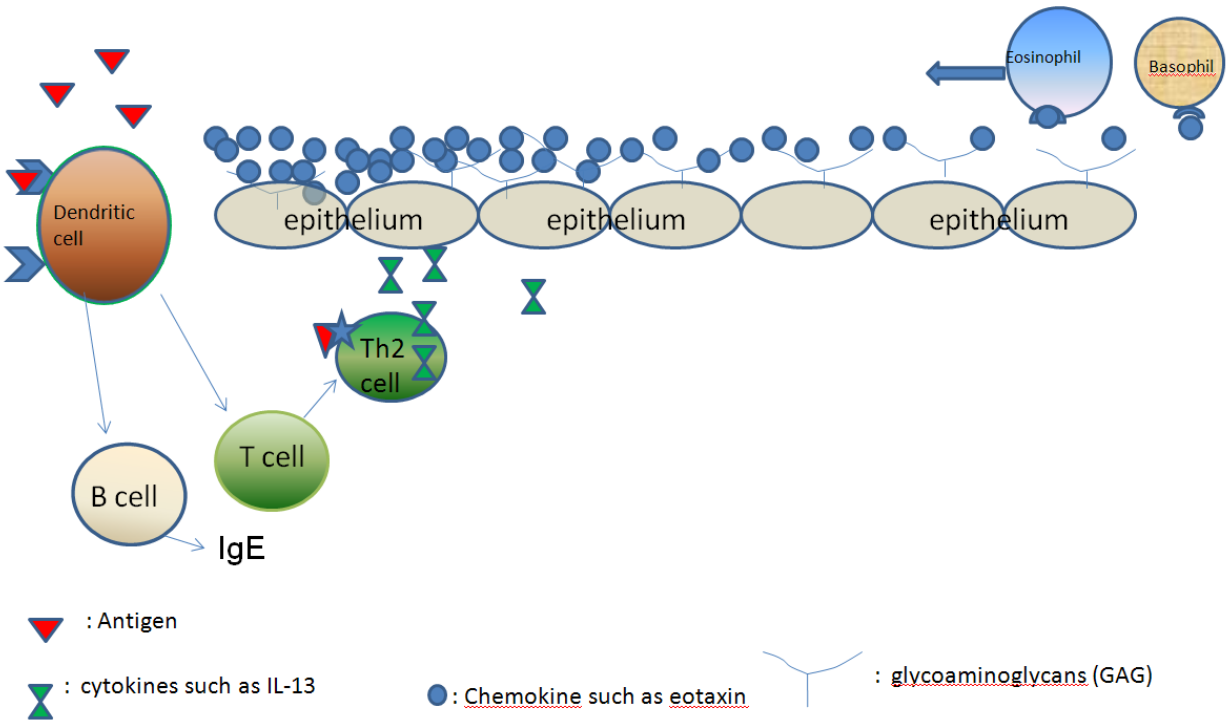

Figure 1.2. An overview of how an antigen initiates the chemotaxis of leukocytes. Immature dendritic cells located in skin, lung, intestine become activated when interacting with antigens such as pathogen or pollen, subsequently move to the lymph node to activate naïve T cells and B cells. T cells become T helper type 2 cells and release chemokines such as IL_13; which induces epithelium to produce inflammatory chemokines like eotaxin. Secreted chemokines establish a concentration gradient by binding to the glycoaminoglycans on the epithelium. Nearby leukocytes (eosinophils, basophils) get activated through its receptors (CCR3) interacting with chemokines. After a variety of physiological and cellular responses such as integrin relocation, activated leukocytes migrate along the chemokine gradient to the infected site.

higher-order oligomers) and monomers. They interact with GAGs as oligomers to form a chemokine gradient with highest concentration at the infected location, and they interact with their receptors on immune cells as monomers. This model is supported by several publications. For example, Harshica Fernando discovered IL-8 forms dimers on binding to GAGs in a variety of *in vitro* and *in vivo* studies, and activates its receptor as a monomer in *in vitro* cell-based assays (13). Additionally, MIP-1β also forms dimers in μM scale concentration; its dimerization ability is strengthened upon binding with GAGs (14). However, the obligate MIP-1β dimer that cannot dissociate to form monomers is unable to bind or activate the MIP-1β receptor CCR5 (15).

Chemokines recruit target cells by interacting with specific receptors called G-coupled protein receptors (GPCR). Currently about 20 chemokine receptors have been identified which are expressed on different leukocyte subsets (16). Chemokine receptors are divided into four families depending on what kind of chemokine they bind: CCR, CXCR, CX3CR and XCR. Generally, CC-chemokines bind to CC-chemokine receptors and control chemotaxis of eosinophils, lymphocytes, monocytes, and basophils. CXC-chemokines tend to interact with CXC-chemokine receptors and regulate neutrophils. The binding pattern between a chemokine and its receptor is both specific and diverse; a chemokine can bind to several different receptors in the same family, and in turn a receptor might interact with a few chemokines. For example, eotaxin has three receptors: CCR2, CCR3, CCR5; CCR5 has 3 different ligands: RANTES, MIP-1α and MIP-1β (17,18). Therefore a leukocyte cell can be activated by several different chemokines since it expresses different types of chemokine receptors on its surface (19, 20).

Chemokine receptors share some common structural properties: they have about 350 amino acids, a short acidic N-terminal end, seven transmembrane domains with three intracellular and three extracellular hydrophilic loops, and an intracellular C-terminus, which is essential for the interaction with G-coupled protein to transfer a signaling cascade. The general binding mechanism of a chemokine and its receptor is as follows: a positively-charged chemokine ligand binds to the acidic N-terminal loops of the receptor, and then the extended N-terminus of the chemokine interacts with some regions of the transmembrane domains, which causes the chemokine receptor to experience conformational change. This activates G-proteins to initiate the down-stream signaling transduction that leads to cell maturation, differentiation and cell migration (21, 22).

Despite their physiological functions in maintaining a healthy immune system, dysfunction of chemokines and chemokine receptors induces an inappropriate inflammation response and causes a variety of diseases including chronic inflammation, asthma, neurological disorders and cancers (23, 24). Currently, therapies for treating chemokine-mediated diseases are generally involved in suppressing the host immune system, which have the risk for secondary infection. Small molecule antagonists for chemokine receptors are also being evaluated in clinical trials for effectiveness. Scientists are also trying to design anti-chemokine drugs to relieve the symptoms of inflammatary diseases. The most effective ones are monoclonal antibodies of chemokines and chemokine receptors; for example, anti-Interleukin-13 monoclonal antibody was found to effectively inhibit asthma progression in mice (25).

Considering the fact that a wide range of chemokines are involved in inflammation, one inflammatory disease might be caused by several chemokines. Since

one type of monoclonal antibody can only specifically inhibit its own corresponding ligand, it's better to design a drug that can bind a variety of chemokines. The vCCI protein is a good candidate that shows the ability to inhibit a wide range of chemokines.

1.3 Viral CC-chemokine inhibitors (vCCI)

Large DNA virus, especially poxviruses and herpesviruses have developed several strategies to interfere or exploit the host chemokine network. The implementation of these strategies relies on the function of viral proteins including chemokine analogs, chemokine receptor analogs and chemokine binding proteins (CKBPs) (26). These proteins disrupt the interactions between chemokines and their receptors, or between the chemokine and GAGs. CKBPs generally show no similarity to any known host proteins and have wide spectrum chemokine-binding ability.

There are three groups of chemokine binding proteins (CKBPs): poxvirus CKBP-I, poxvirus CKBP-II and herpesvirus CKBP-III. The CKBP-I proteins are believed to interact with the GAG-binding regions of chemokines (27). CKBP-III proteins are found to bind to the receptor-binding areas of chemokines (28). CKBP-II proteins share the feature of binding to many CC chemokines with high affinity (picomolar to nanomolar scale), and show weak binding to chemokines from other chemokine families (29).

vCCI belongs to CKBP-II proteins which is encoded by poxvirus. The name vCCI (Viral CC Chemokine Inhibitor) comes from its feature of inhibiting the function of CC chemokines. It was found by Burns et.al that poxvirus vCCI preferentially bind most CC chemokines, including eotaxin, MCP-1, MIP 1β, with high affinity, based on the

screening results of more than 80 test chemokines. Only a few CC chemokines along with all CXC, C, CX3C chemokines do not bind to vCCI (30).

CC chemokines are pro-inflammatory proteins, so binding to CC chemokines, as vCCI does, implies the potential to inhibit the inflammatory diseases, such as asthma. Some publications have shown the positive results of vCCI relieving inflammatory symptoms. For example, Reading et.al found out that vaccinia vCCI greatly reduced the number of infiltrating cells in the lungs of the experimental mice (31); Additionally, monkeypox virus vCCI was shown to inhibit relapsing Experimental Autoimmune Encephalitis (EAE) in mice (32).

Sequence alignment shows vCCIs share 40%-95% identity and all have the same number and pattern of conserved cysteines. Despite varying similarities, vCCI proteins exhibit very similar *in vitro* capabilities to block CC-chemokine signaling functions. This indicates that vCCI proteins share similar structures and bind to chemokines with similar mechanisms (33). The first vCCI structure was from cowpox and was solved by X-ray crystallography (34). vCCI has a unique structure consisting of 240 amino acids shown in figure 1.3, which shows no similarity to any known mammalian receptors, but has distant resemblance to the collagen-binding domain of *Staphylococcus aureus* adhesion (34). This unique vCCI structure is a β-sandwich fold containing two short α-helices, several loops and two parallel β-sheets. β-sheet I is composed of seven antiparallel β-strands, and its access to the solvent is blocked by two extended loops; β-sheet II is accessible to solvent, and several negatively-charged residues on the surface of β-sheet II were predicted to bind to the positively charged chemokines.

Considering the importance to treat the popularity of inflammatory diseases, any contribution that leads to an understanding of the binding mechanism of CC chemokines

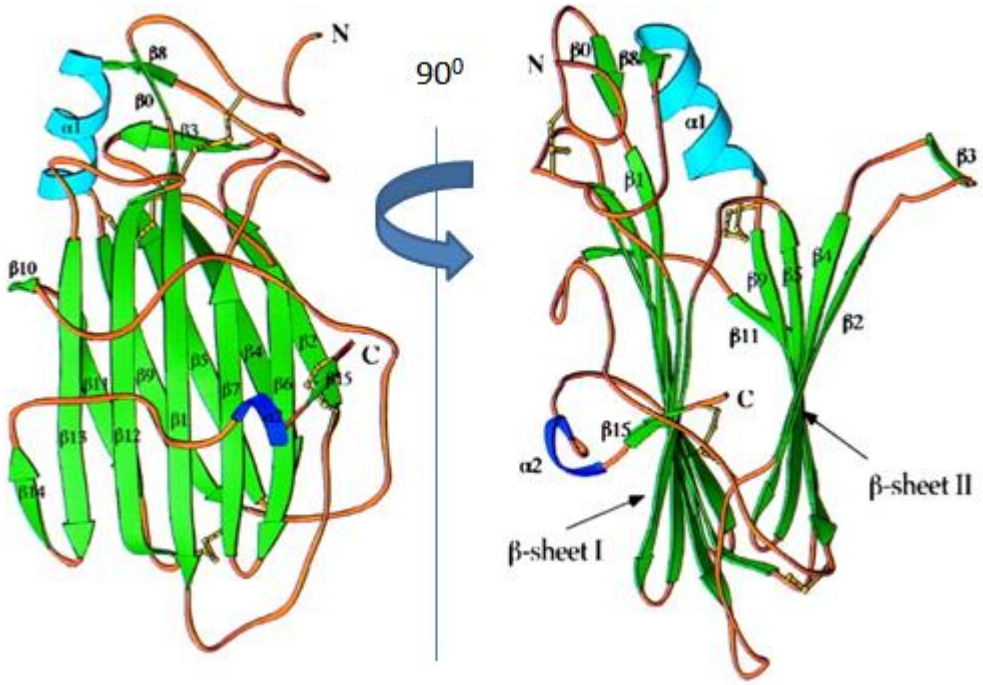

Figure 1.3 (Copied from reference 34 by Burns et al.). Ribbon diagram of vCCI structure of compox virus. The vCCI structure shows a β-sandwich fold containing two short α-helices and two parallel β-sheets. While β-sheet I has two extended loops that can block the access of the solvent, the β-sheet II region exposed to solvent posses several negatively-charged residues and is predicted to bind to positively charged chemokines.

interacting with vCCI would be valuable. By now there are a few publications showing the binding information of CC chemokines. For example, a binding analysis of MCP-1 was conducted through site-directed mutagenesis and two detection techniques: ELISA and surface plasmon resonance. Despite the inconsistency of the two data sets acquired from the two techniques, it's still revealed that positively-charged residues contribute the most to its high vCCI- binding affinity. Additionally most of the same residues are also used to bind to receptor CCR2B (36, 37). To figure out the comprehensive mechanism of vCCI binding a variety of CC chemokines, more investigations need to be done to figure out if the counterparts of those residues important for MCP-1 binding to vCCI on other CC-chemokines have similar influence on binding to vCCI.

Currently, there is only one publication describing the binding mechanism from the angle of both vCCI and CC chemokine, which was a structural study of the complex composed of vCCI and a chemokine (MIP-1β) carried out in our lab with the technique NMR (37). The binding mechanism is shown in Figure 1.4. Analysis of this complex reveals that the binding stoichiometry of vCCI:MIP-1β is 1:1, the vCCI-binding site of MIP-1β overlaps with regions used by the chemokine to bind its receptor, to interact with GAG and to form dimers. It also confirmed the prediction that negatively-charged residues of β-sheet II in vCCI make the dominant contact with positively-charged residues of chemokine. But more effort is needed to elucidate which residues play a key role in binding and how the negatively-charged flexible loop in vCCI between strand β2 and β3 impacts the binding of chemokines.

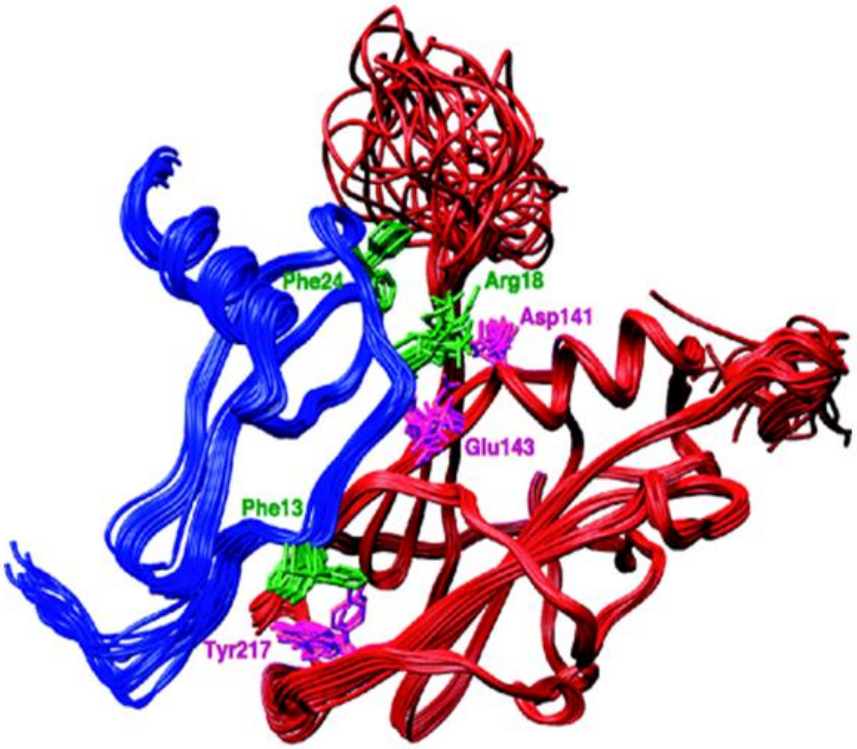

Figure 1.4 (copied from reference 37 by Zhang et al.). Binding mechanism between vCCI and MIP-1β. vCCI backbone is red with selected side chains colored in pink; MIP-1 backbone is blue with selected side chains shown in green. This complex structure reveals that the binding stoichiometry of vCCI:MIP-1β is 1:1, the vCCI-binding site of MIP-1β overlaps with regions used by the chemokine to bind its receptor, to interact with GAG and to form dimers. It also confirmed the prediction that negatively-charged residues of β-sheet II in vCCI make the dominant contact with positively-charged residues of chemokine.

This thesis presents the binding mechanism between eotaxin and vCCI. Chapter 2 describes the development of a sensitive detection technique (fluorescence anisotropy) and the investigation of binding residues of eotaxin. Chapter 3 addresses the making of several vCCI variants, and binding results of several vCCI variants to eotaxin. Chapter 4 talks about the making of a crystal of the complex, vCCI:eotaxin. Chapter 5 is the conclusion.

Chapter 2

Investigation of the Essential Binding Residues of Eotaxin Through Mutagenesis and Fluorescence Anisotropy

2.1 Introduction

CC Chemokines are major factors for the inflammatory diseases. They share many features. For example, they are small proteins (8-14 kDa); share 25 – 50% identity; they all possess four conserved amino acids that are important for creating their 3-dimensional structure with unique Greek key shape, which form 2 disulfide bonds. Two cysteines are located adjacently in the N-terminus. The first cysteine connects to the third one in the 30s loop, the second cysteine interacts with the fourth one in the 50s loop. Each CC Chemokine's structure starts with an unstructured N-terminus and a long flexible loop known as the N-loop, followed by a single-turn helix, three antiparallel β-strands and a C-terminal α-helix. As for the function of different parts of chemokines, generally the N-loop region is used to bind with the receptor, while the unstructured N-terminus is involved in receptor activation, and a 40's loop and C-terminal helical region are used in GAG (Glycosaminoglycans) binding (7, 8). More specifically, there are several conserved residues located in those binding areas of CC chemokines which might be involved in interacting with the other target protein of this thesis, vCCI (Figure 2.1). Using MCP-1 as a reference, for those CC chemokines that can tightly binding to vCCI, their vCCI-binding pattern is as follows: Position 13 is usually a hydrophobic residue, position 18 is positively charged. There is at least one positively charged amino acid in the 24/45 position. If they are lacking a positively charged residue in both 24 and 45

position, then position 46 needs to be positively charged. This pattern was verified by Zhang et al. using NMR structure determination to show that Phe13, Arg18 of MIP-1β are used to interact with vCCI, most probably K45 and R46 also contribute to the vCCI-binding (37). It was also found in MCP-1 by Seet et al. and Beck et al. that Phe13, Arg18 and Arg24 are determinants for MCP-1 to bind vCCI (35, 36). Those binding determinants are shown in figure 2.2. In contrast, for those chemokines that show low or no affinity to vCCI, such as MDC, they do not show this pattern.

Because eotaxin binds vCCI with high affinity, a very sensitive method is required that can monitor the binding interaction at low concentration, such as Surface Plasmon Resonance (SPR), or scintillation proximity assay. These techniques either need particular instruments and complex processing software or radioactive chemicals, along with a complex procedure to prepare samples that might damage the structure of proteins. Relative to those methods, fluorescence anisotropy is an operation-friendly method with high sensitivity that monitors fluorophores like fluorescein-5-maleimide which emits detectable signal even at a nanomolar concentration. Therefore, this project develops the use of fluorescence anisotropy to measure the binding between chemokines and vCCI. In this project, fluorescein-5-maleimide is attached to Cys75 at the end of C-terminus of the CC chemokines since this position is not involved in the binding interaction with vCCI. The main challenging part is to actually label the protein with fluoresceine dye. Aside from that, the binding system is in solution which is easy to prepare and to collect data. Figure 2.3 describes the mechanism of fluorescence anisotropy. In this method, the fluorophore, which is attached to the smaller protein of a binding system, is excited by a

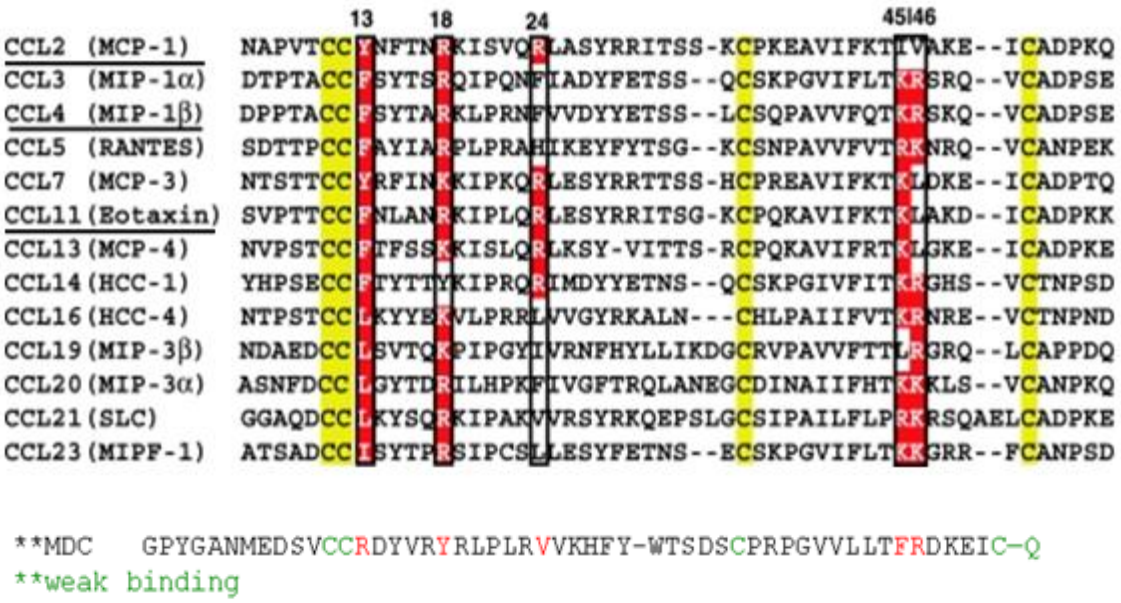

Figure 2.1 (from reference 37 by Zhang et al). Sequence alignment of the human CC chemokines with high affinity towards vCCI. Conserved cysteine residues are highlighted in yellow. Positions highlighted with red indicate residues that likely confer high-affinity binding to vCCI. The numbering is according to the MCP-1 sequence.

**: represents weak binding.

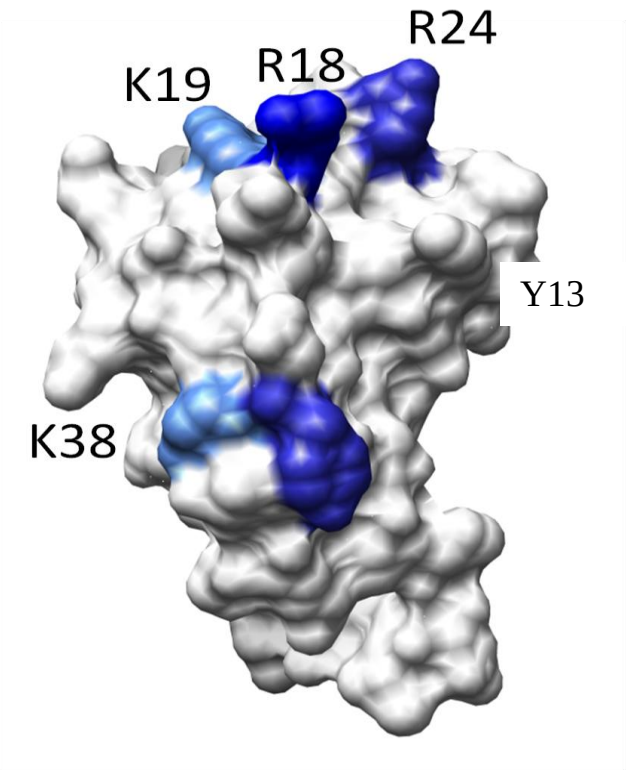

Figure 2.2 (from reference 36 by Beck et al). The vCCI-binding determinants of MCP-1. The color labeled residues are involved in vCCI-binding analyzed by mutation studies. Dark blue represents strong contribution of binding; light blue indicates moderate contribution of binding.

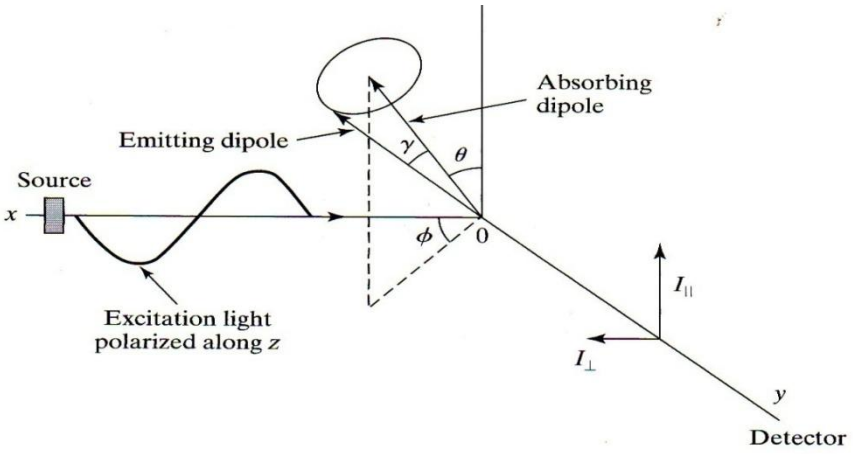

Figure 2.3 (from reference 38 by van Holde. et al.). The mechanism of fluorescence anisotropy. Fluorophore, which is attached to the smaller protein of a binding system, is excited by a polarized light source and emits partially depolarized light. This depolarization is caused by the difference between the emitting dipole and the absorbing dipole, partially as a result of the fast rotation of fluorophore in the solution. Unbound Fluorophore-attached protein rotates quickly which causes obvious depolarization shown as small anisotropy; however, when bound to a bigger protein, the resulted complex rotates slowly and causes less depolarization resulting in a bigger anisotropy value.

polarized light source and emits partially depolarized light. This depolarization is caused by the difference between the emitting dipole and the absorbing dipole, partially as a result of the fast rotation of fluorophore in the solution. Unbound Fluorophore-attached protein rotates quickly which causes obvious depolarization revealed as a small anisotropy value. However, when bound to a bigger protein, the resulting complex rotates slowly and causes less depolarization resulting in a bigger anisotropy value.

Therefore, a binding reaction can be quantitatively monitored by measuring the change in fluorescence anisotropy of a labeled chemokine as binding partner vCCI is titrated into solution.

2.2 Materials and methods

Cloning and expression of recombinant eotaxin-C75. In order to label the eotaxin with fluorescein dye that reacts with the thiol group, an extra cysteine residue was added to the C-terminus of eotaxin by inserting the cysteine codon into the gene of eotaxin through PCR engineering. The gene encoding the eotaxin-C75 was made from commercial plasmid with eotaxin in pET 28 vector, using primers specific for eotaxin which also contained a 6* -histidine tag (underlined region) and restriction sites for NcoI (GCCGCGCCATGGCATCACCACCACCACCATGCGGGCCCACGTGGTCCAGCT-TCTGTTCCGACTACC) and XhoI (GGAGCACTCGAGTCAGCACGGTTTCGGGGT-CGGAGATTT CTG). The resulting product was cloned into pET-15b vector for expression. Rosetta 2 (DE3) cells were transformed with the pET-15b plasmids. Bacteria was grown in LB medium for ^{14}N eotaxin-C75 protein expression, or in M9 minimal medium containing $^{15}NH_4Cl$ as the sole nitrogen resource for ^{15}N- labeled

protein. Ampicillin was added to both types of media at a final concentration of 1 mg/L as selection reagent. IPTG was added into the culture at final concentration of 1 mM when the absorbance at 600 nm was in the range 0.6 – 0.9. Cells were harvested by centrifugation with 6000 rpm after 4 hours of induction, cell pellet was resuspended in about 30 ml 20 mM pH 8.0 Tris-HCl with 50 mM NaCl. Benzamidine was added to a final concentration of ~ 1 mg/ml to inhibit the degradation effect of protease. Resuspended Cells were processed twice through French Press at 12,000 psi. The lysate was centrifuged at 15,000 x g at 4 °C for 1 hour. The supernatant portion contained most of the eotaxin-C75 protein was added with 5 M NaCl to a final concentration of 500 mM NaCl. The supernatant was passed through a nickel column to separate the tagged eotaxin-C75 from most of the junk material. There were two elution buffer agents: (1) pH 8.0 20mM Tris-HCl with 50 mM NaCl and 5 mM imidazoe, (2) pH 8.0 20mM Tris-HCl with 50 mM NaCl and 500 mM imidazole. The tagged eotaxin-C75 that bound to the nickel column was then eluted out during a gradient-washing process. The peaks containing the eotaxin-C75 were collected and dialyzed twice in pH 8.0 20 mM Tris-HCl with 50 mM NaCl. The first dialysis was done in 4 hours at room temperature or overnight at 4 °C. During the second dialysis, 1.5 µl 20,000 unit cleavage enzyme, Thrombin, was added in the dialyzing bag, then was let to stand by overnight at room temperature. The cutting reaction was not stopped until all His-tag was removed from the eotaxin-C75 which was monitored by sodium dodecyl sulfate polyacrylamide gel electrophoresis (SDS-PAGE). After Thrombin cleavage, the tag-free eotaxin-C75 was prepared for reverse-phase chromatography by addition of trifluoroacetic acid to adjust the pH to about 2, and acetonitrile to a final concentration of 10% (v/v). The sample was

loaded onto a C4 reverse-phase column and eluted by an acetonitrile gradient. The fractions containing tag-free eotaxin-C75 were confirmed by SDS-PAGE and quantified with the following equation, concentration of protein = [O.D. ÷ (extinction coefficient at 280 nm * 1 cm)], the extinction coefficient of eotaxin-C75 is 8700 $cm^{-1}M^{-1}$. The final step is to lyophilize the eotaxin-C75 and store it.

Eotaxin variants preparation: The gene of human eotaxin integrated in the pET-28a vector was commercially acquired (Invitrogen, Carlsbad, CA). Four single mutation eotaxin variants (F11A eotaxin, R16A eotaxin, R22E eotaxin, K47A eotaxin) and three double mutation eotaxin variants (R16AR22A eotaxin, R22AK44A eotaxin, R22EK44A eotaxin) were made through Quik Change site directed mutagenesis (Stratagene, La Jolla, CA) using wild type eotaxin as template along with proper primers containing target mutation. Wild type eotaxin plasmid was transformed into BL21(DE3), eotaxin mutant plasmids were transformed into Rosetta 2 (DE3). Unlabeled and 15N-labeled proteins of eotaxin variants were expressed and purified through the same protocol described in the part, *cloning and expression of recombinant eotaxin-C75*.

vCCI preparation: The gene encoding rabbit poxvirus vCCI was kindly given by Professor Richard Moyer of University of Florida. The DNA was cloned into pPIC9K vector, then transformed into *Pichia pastoris* strain SMD1168 (Multiple-copy Pichia Expression kit, Invitrogen, Carlsbad, CA). Transformed Yeast cells were grown at 28 °C in pH 6.0 minimal glucose media, when O.D. value was between 2 – 6, cells were centrifuged with 2000 rpm 10 mins, cell pellet was resuspended in minimal methanol media with $^{14}NH_4SO_4$ (or $^{15}NH_4SO_4$ for 15N labeled protein) as the sole nitrogen

resource, along with methanol as the sole carbon resource and induction reagent. During the induction process, methanol was maintained at ~0.2% by adding 1 ml per 500 ml every 12 hours. The expression of vCCI throughout the induction process was monitored by sampling the supernatant of 200 µl culture containing secreted vCCI and running it on the SDS-PAGE. After 48 – 72 hours of induction, the *Yeast* culture was harvested and centrifuged to get the supernatant, the remaining cells in the supernatant was removed by filtration with 2 µm filter. The supernatant was diluted by two-fold with water to reduce the concentration of salt, and then purified by an anion exchange column with a gradient salt washing. The fractions containing vCCI were collected and concentrated using the Amicon concentrators (Millipore, Billerica, Massachusetts) to about 1 ml, and then further purified by G75 size exclusion column. The fractions of vCCI protein were concentrated with Amicon concentrators to certain concentration range depending on the future application. For titration experiments between vCCI and eotaxin, the concentration was around 100 µM; for NMR spectrometry, the concentration was either ~ 100 µM to just check folding status or above 800 µM for sequence-specific assignment. The concentrated vCCI was aliquoted into 100 µl portions, and stored at -80°C for future usage.

NMR Spectroscopy. Two-dimentional NMR spectra data were collected to test if the proteins are well folded; to find out if the labeling reaction influence the natural structure of eotaxin; to very the target residue of site-directed mutation was succesful; to make sure there is binding interaction between eotaxin and vCCI. Spectra were recorded at 25 or 37 ˚C on one of Varian Inova 500, 600 and Bruker 600 NMR spectrometers. NMR data

were processed using NMRPipe (39). Methyl resonance of DSS was used as reference to calculate the chemical shifts of proton and nitrogen,

Labeling Eotaxin-C75 with Fluorescein-5-maleimide. Eotaxin-C75 powder was dissolved in pH7.0 buffer system composed of 20 mM Potassium phosphate and 50 mM NaCl buffer, adjusted the concentration of eotaxin-C75 to be in the range of 100 – 200 μM (part one of labeling system). For part two of the labeling system, Fluorescein-5-maleimide was dissolved in Dimethylformamide (DMF) with the final concentration to be equal of 20 fold of the concentration of eotaxin-C75 in part one of labeling system. Part two of labeling system was dropwise added into part one of labeling system with mixture. The labeling system was let stand for 3 hours. To remove excessive fluorescein-5-maleimide and unlabled eotaxin, two purification techniques were utilized. The first one was G25 size exclusion column which was used to roughly remove most of the unreacted fluorescein-5-maleimide. The second purification step was using C4 reverse-phase column to separate labeled eotaxin-C75 from unlabeled eotaxin-C75. Figure 2.4 shows the elution spectrum of C4 reverse-phase column, and the purification performance monitored by SDS-PAGE. The images show most of the eotaxin-C75 was labeled with fluorescein-5-maleimide, the labeled eotaxin-C75 was separated from the unlabeled one after purification of C4 reverse-phase column. The labeling yield of the product eluted from the G25 size column was ~200% which indicates that there were free fluorescein-5-maleimide co-existing with eotaxin-fluo. The labeling yield of the product eluted from the C4 column was 84% which indicate eotaxin-fluo was well purified.

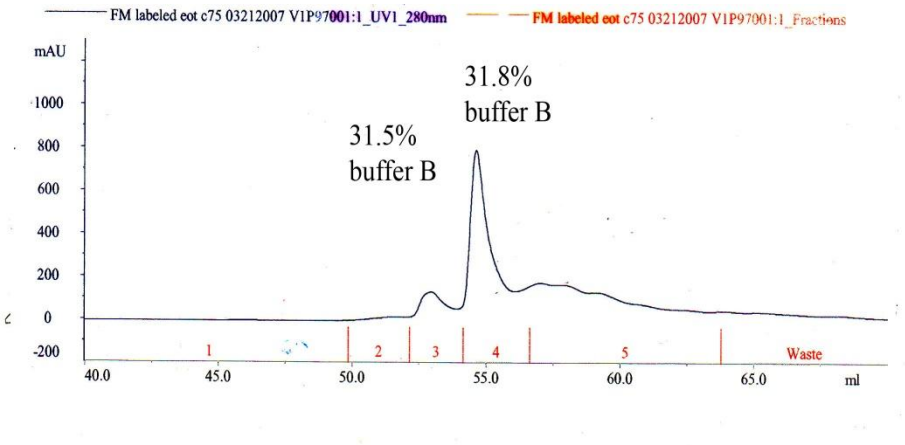

Figure 2.4.1. The 2nd-step purification HPLC spectrum of eotaxin-C75-fluo eluted from G25 size exclusion column

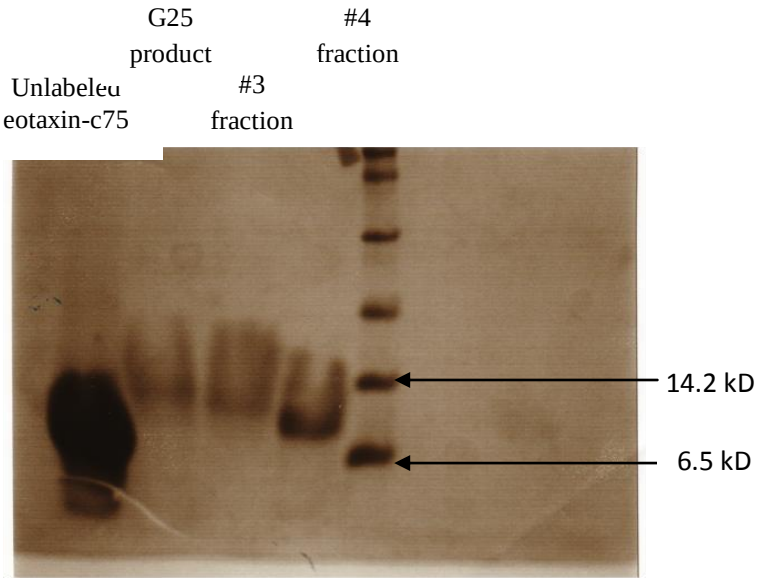

Figure 2.4.2. Coomassie staining image of SDS-PAGE of the products eluted from size column and from C4 column

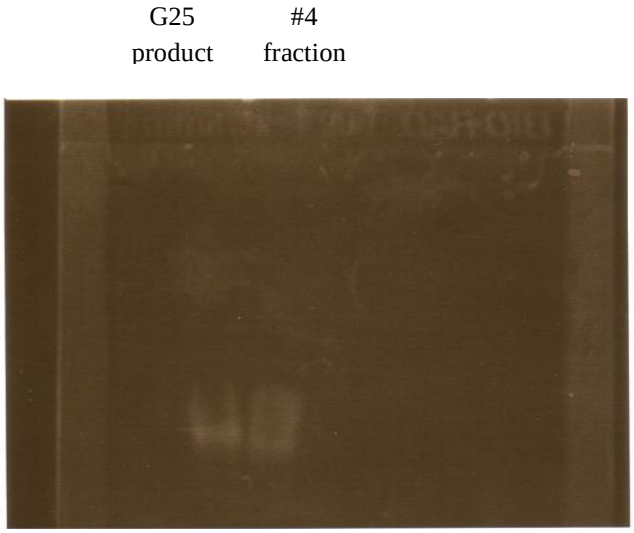

Figure 2.4.3. UV-image of SDS-PAGE of the products eluted from size column and from C4 column

The concentration of labeled eotaxin-C75 (eotaxin-fluo) was determined by coomassie plus assay (Pierce Protein Research Products, Rockford, IL) with eotaxin-C75 as the standard. First, the concentration of eotaxin-fluo was estimated using nanodrop spectrophotometer (NanoDrop Products, Wilmington, DE), then 3 parallel 0.5 ml samples of eotaxin-fluo with concentration of 4 μg/L was prepared. At the same time, a series of standard concentrations (eotaxin-c75), from 0.5 to 8 μg/L, were prepared in 0.5 ml. After that, 0.5 ml coomassie plus reagent was added in both samples an standards, and mixed well. After 10 minutes of reaction, samples were determined at wavelength of 595 nm. A linear equation was acquired through curve fitting program using the data of standards. The concentration of eotaxin-fluo was calculated using the acquired equation.

2.3 Results

Before putting any effort to investigate the binding residues of eotaxin, the first step of this project was to demonstrate that the CC chemokine (eotaxin in this project) binds to vCCI. This was shown by comparing the ^{15}N heteronuclear single quantum correlation (HSQC) spectrum of the unbound eotaxin and bound eotaxin in complex with vCCI (Figure 2.5). Every peak of the HSQC spectrum corresponds to one N-H group of the amino acids of the protein. Addition of unlabelled vCCI into ^{15}N-labeled eotaxin caused noticeable changes of some peaks in the spectrum, indicating interaction between these two proteins. To get the spectrum exclusively from the bound eotaxin, more than one equivalent of vCCI was added in ^{15}N-labeled eotaxin to decrease the peaks from eotaxin dimerization and unbound eotaxin. Drastic spectral changes were detected in

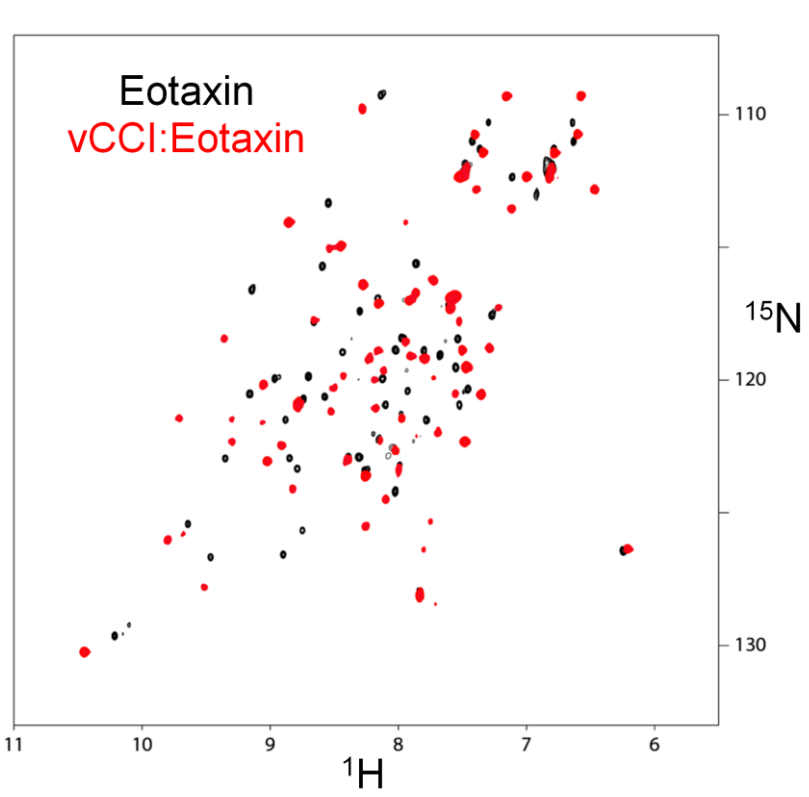

Figure 2.5. Interactions between eotaxin and vCCI shown by NMR spectrum. Overlay of ^{15}N heteronuclear single quantum correlation (HSQC) spectrum of unbound (black) and bound (red) ^{15}N-labeled eotaxin. vCCI shows no peaks since it is not labeled with ^{15}N. 25 °C, pH5.0, concentration of eotaxin was 200 µM.

bound eotaxin (eotaxin :vCCI), indicating there were interactions between eotaxin and vCCI.

As mentioned, in order to add a fluorephore to eotaxin, a Cys was appended to the end of the protein at position C75. This extra cysteine might interact with the existing four cysteines of eotaxin and change the structure of eotaxin. To test this, an ^{15}N HSQC spectrum was measured. This figure shows few changes, indicating eot-c75 is near wild type in structure (Figure 2.6.1). After the process of labeling, it's necessary to find out if the eotaxin-fluo still maintains its original structure which was determined by NMR. Figure 2.6.2 shows the ^{15}N HSQC spectrum of the unlabeled eotaxin-C75 and eotaxin-fluo. Figure 2.6 indicates that eotaxin-fluo keeps the same conformation as the intact eotaxin.

To determine whether particular amino acids are important in binding vCCI, several mutants of eotaxin were prepared (Table 2.1). Before the conclusion was made that it's the residue replacement, such as alanine replacing arginine, not the structure change that caused obvious change of binding affinity, these eotaxin variants were checked by NMR to make sure their structures are similar as the intact eotaxin. ^{15}N HSQC spectrum of the eotaxin were acquired and compared with wild type eotaxin (Figure 2.7). The HSQC spectra of F11A eotaxin, R16Aeotaxin, R22E eotaxin, K44A eotatxin, K47A eotaxin, R16AR22E eotaxin showed a similar peak pattern as that of wt eotaxin; only the peaks of mutated residues were gone as expected. The HSQC spectra of R22EK44A eotatxin, R22AK44A eotaxin did not match the spectrum of wt eotaxin very well although most peaks overlapped. In these cases it appears that there were some

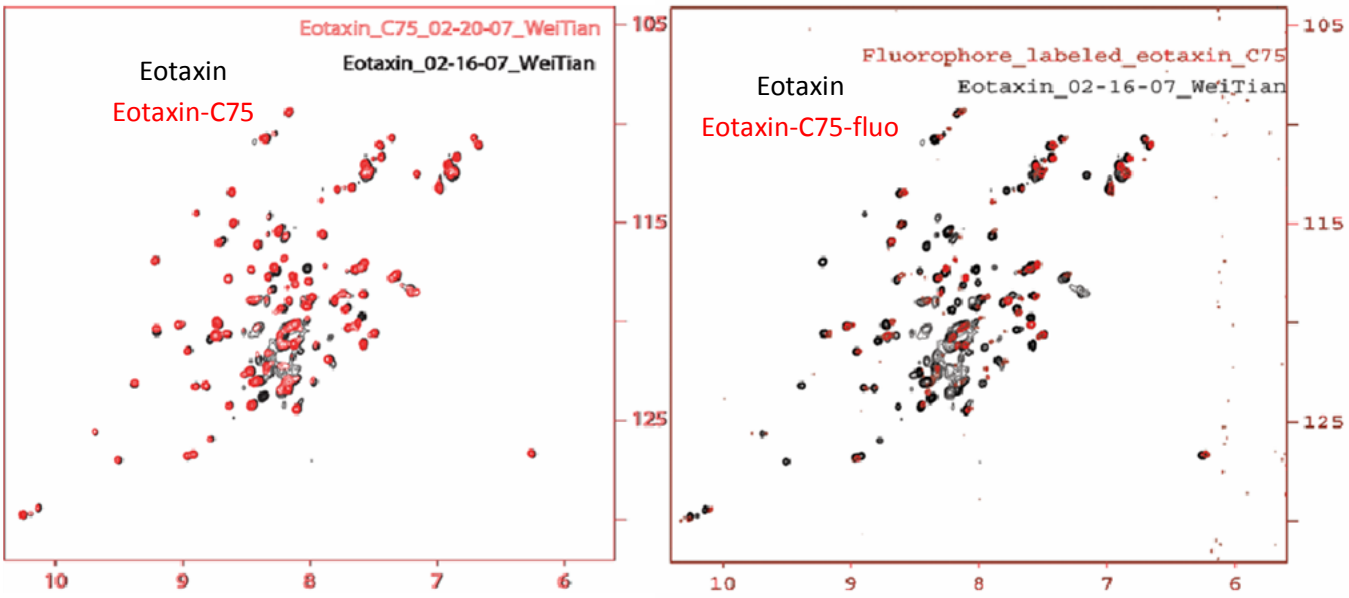

Figure 2.6.1. Overlay of wild type eotaxin (black) and eotaxin-C75 (red). pH: 5.0; concentrations of wild type eotaxin and eotaxin-c75 are individually 200 μM.

Figure 2.6.2. Overlay of wild type eotaxin (black) and fluorophore-labeled eotaxin-C75 (red). pH: 5.0; concentrations of wild type eotaxin and fluorophore-labeled eotaxin-c75 are individually 200 μM and 50 μM.

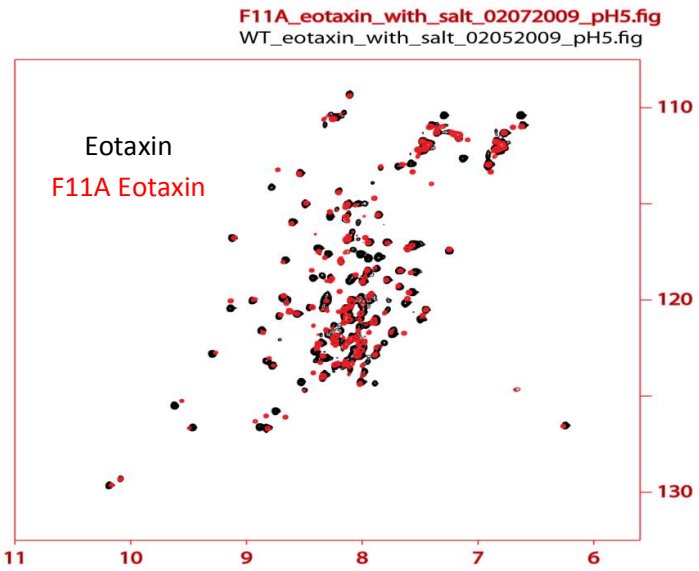

Figure 2.7.1. Overlay of wild type eotaxin (black) and F11A eotaxin (red).

pH: 5.0; concentrations of wild type eotaxin and F11A eotaxin are individually ~ 200 μM.

Chemical shifts of N-H group of F11 of eotaxin are not available in the NMR data bank.

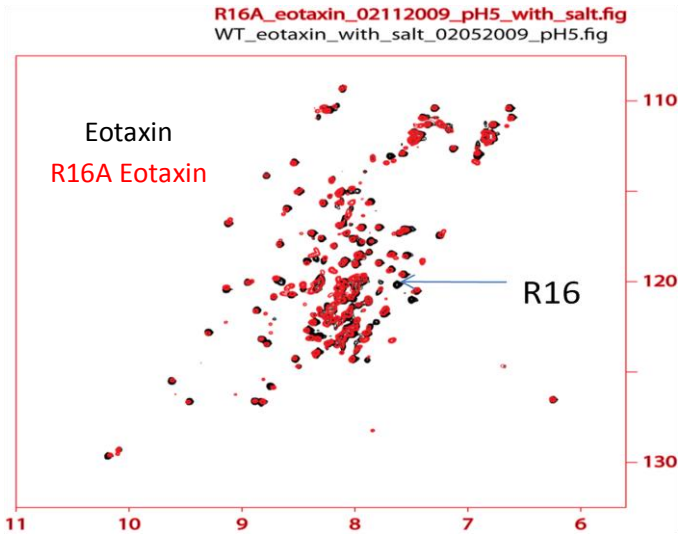

Figure 2.7.2. Overlay of wild type eotaxin (black) and R16A eotaxin (red). The peak of R16 is gone in R16A eotaxin. pH: 5.0; concentrations of wild type eotaxin and R16A eotaxin are individually ~ 200 μM. Chemical shifts of N-H group of R16 of eotaxin are as the following: N: 120.01ppm, H: 7.63ppm.

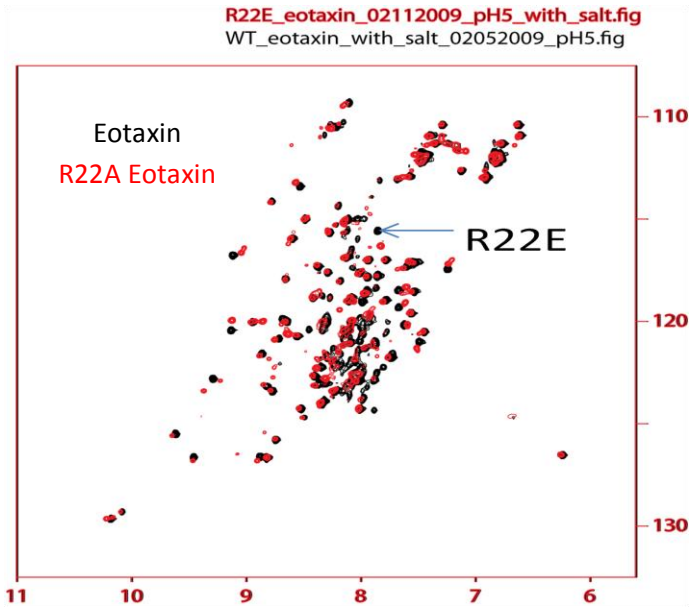

Figure 2.7.3. Overlay of wild type eotaxin (black) and R22E eotaxin (red). The peak of R22 is gone in R22E eotaxin. pH: 5.0; concentrations of wild type eotaxin and R22E eotaxin are individually ~ 200 μM. Chemical shifts of N-H group of R22 of eotaxin are as the following: N: 115.45ppm, H: 7.87ppm.

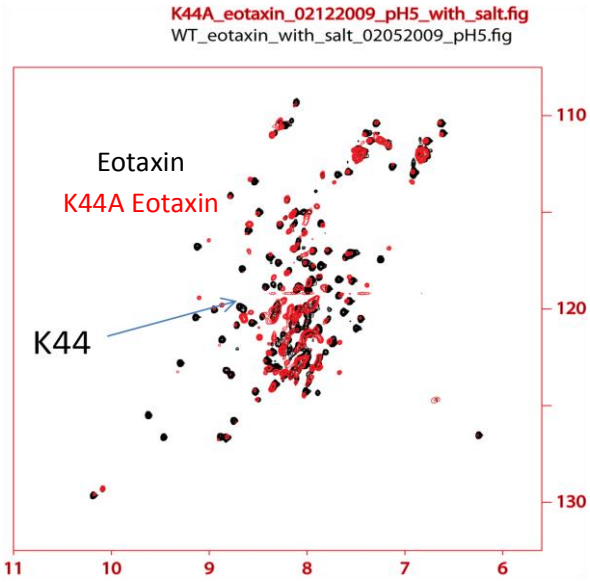

Figure 2.7.4. Overlay of wild type eotaxin (black) and K44A eotaxin (red). The peak of K44 is gone in K44A eotaxin. pH: 5.0; concentrations of wild type eotaxin and K44A eotaxin are individually ~ 200 μM. Chemical shifts of N-H group of K44A of eotaxin are as the following: N: 119.83ppm, H: 8.74 ppm.

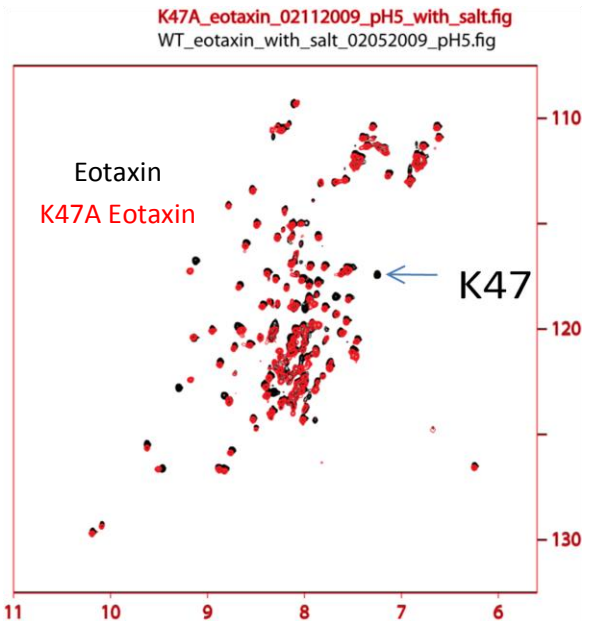

Figure 2.7.5. Overlay of wild type eotaxin (black) and K47A eotaxin (red). The peak of K47 is gone in K44A eotaxin. pH: 5.0; concentrations of wild type eotaxin and K47A eotaxin are individually ~ 200 μM. Chemical shifts of N-H group of K47A of eotaxin are as the following: N: 117.05ppm, H: 7.26 ppm.

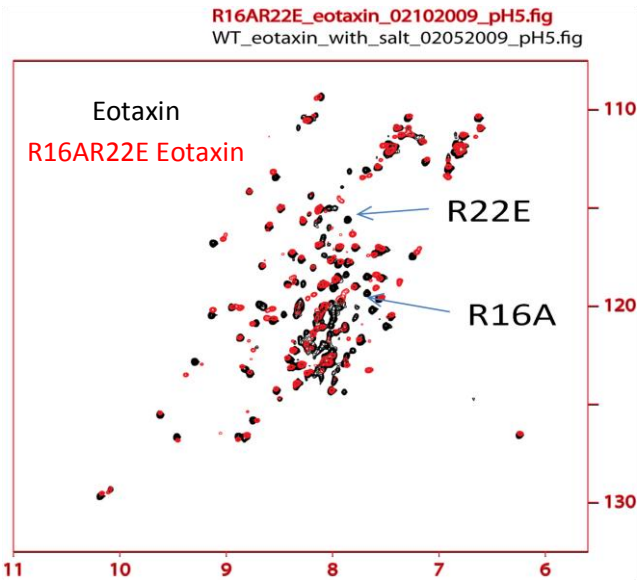

Figure 2.7.6. Overlay of wild type eotaxin (black) and R16AR22E eotaxin (red). The peaks of R16 and R22 are gone in R16AR22E eotaxin. pH: 5.0; concentrations of wild type eotaxin and R16AR22E eotaxin are individually ~ 200 μM. Chemical shifts of N-H groups of R16 and R22 of eotaxin are as the following: N of R16: 120.01 ppm, H of R16: 7.63 ppm; N of R22: 115.45 ppm, H of R22: 7.87 ppm.

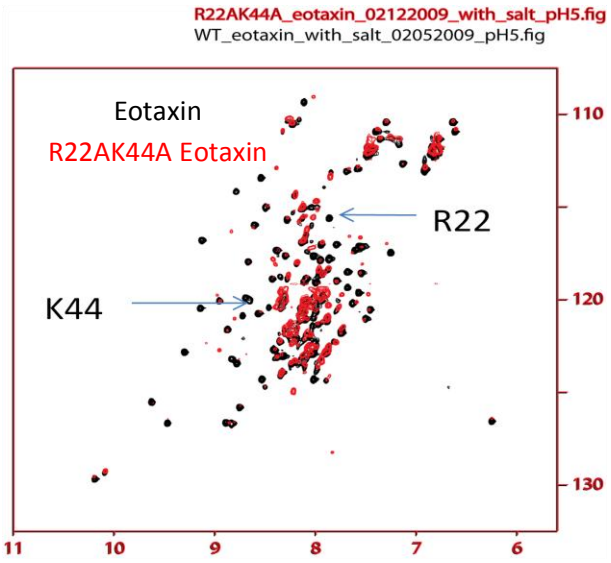

Figure 2.7.7. Overlay of wild type eotaxin (black) and R22AK44A eotaxin (red). The peaks of R22 and K44 are gone in R22AK44A eotaxin. pH: 5.0; concentrations of wild type eotaxin and R22AK44A eotaxin are individually ~ 200 μM. Chemical shifts of N-H groups of R22 and K44 of eotaxin are as the following: N of R22: 115.45 ppm, H of R22: 7.87 ppm; N of K44: 119.83 ppm, H of K44: 8.74 ppm.

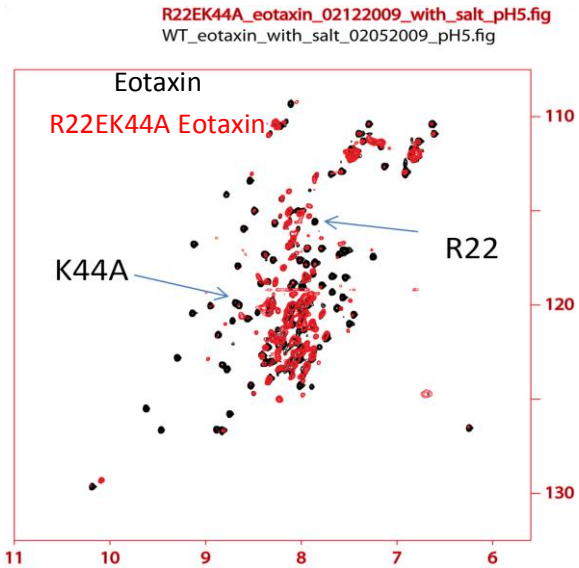

Figure 2.7.8. Overlay of wild type eotaxin (black) and R22EK44A eotaxin (red). The peaks of R22 and K44 are gone in R22EK44A eotaxin. pH: 5.0; concentrations of wild type eotaxin and R22EK44A eotaxin are individually ~ 200 μM. Chemical shifts of N-H groups of R22 and K44 of eotaxin are as the following: N of R22: 115.45 ppm, H of R22: 7.87 ppm; N of K44: 119.83 ppm, H of K44: 8.74 ppm.

unstructured peptides or parts of the mutated eotaxin coexisting with the well-folded proteins. The chemical shift information of eotaxin was acquired in the website of NMR data bank, http://www.bmrb.wisc.- edu/, the entry code is 4155.

After all materials were prepared, titration experiments were carried out to calculate the binding affinities between eotaxin variants and vCCI. The first step in this procedure was to determine the lowest concentration of eotaxin-fluo at which sufficient signal intensity was produced. After a series of tests, 8 nM of eotaxin-fluo was chosen because it emitted around 20,000 photon counts with an acceptable standard deviation.

In this project, Free eotaxin-fluor (8.6 kD) rotates quickly which causes even more depolarization shown as small anisotropy; however, eotaxin-fluor:vCCI complex (35 kD) is much bigger, so it rotates slowly and causes less depolarization resulting in a bigger anisotropy value. The anisotropy change was around 0.055 between free eotaxin-fluo and vCCI-bound eotaxin-fluo, with the anisotropy value of free eotaxin-fluo to be ~ 0.165. The negative control (50 nM bovine serum albumin) did not show obvious anisotropy change, indicating no binding to eot-fluo. The data set of a series of titration of vCCI stock into eotaxin-fluo solution was collected (shown in Figure 2.8) and the binding affinity (K_d) was acquired through curve fitting program (described in supplemental material). The K_d of eotaxin-fluo binding vCCI is ~0.7 nM (Table 2.1).

To avoid the tremendous work of labeling every eotaxin mutant with fluoroscein-5-maleimide, competition binding assays were carried out. A certain amount of eotaxin-fluo was combined with vCCI. Then mutant eotaxin was titrated into the solution to

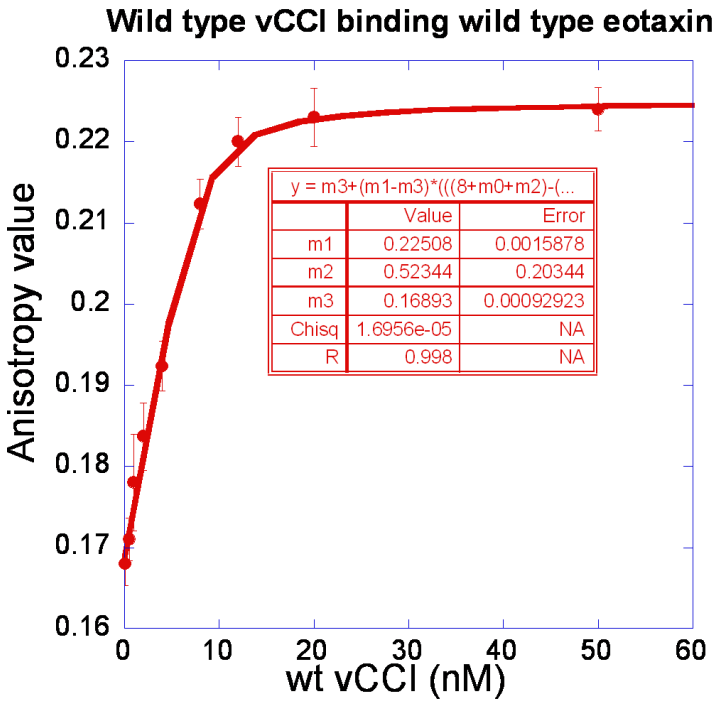

Figure 2.8. Titration of eotaxin-fluo with vCCI monitored by fluorescence anisotropy.

compete with eot-fluo to bind to vCCI, and the resulting change of anisotropy as the eot-fluo was measured. Data were collected and processed using the Kaleidagraph program to aquire the dissociation constant (K_d) of each eotaxin mutant (Figure 2.9, Table 2.1). It should be mentioned that the acquired K_d value (~0.7 nM) derived from the competition assay is far below the concentration of eotaxin-fluo in the binding system (8 nM). Since there are no data points near the K_d value, the determined K_d can only be an estimate. At the same time, half maximal inhibitory concentration values (IC_{50}) were also calculated to compare the binding difference between the eotaxin mutants and wild type eotaxin (Table 2.2).

Table 2.1 and 2.2 also list the relative binding difference between eotaxin mutants and wild type eotaxin individually based on K_d and IC_{50} values, which are shown in columns in Figure 2.10 and Figure 2.11. The two sets of data of relative binding difference mostly match each other. Wild type eotaxin showed the most efficient competition (0.69 nM Kd) to release eotaxin-fluor, which verified the NMR result that eotaxin- fluor has nearly identical structure to eotaxin. Based on the structural information of MIP-1β:vCCI, eotaxin Arg22 (Arg24 in MIP-1β) and Lys44 (Lys45 in MIP-1β) are close to the acidic loop of vCCI. Therefore, changes of the two positively-charged residues would both decrease eotaxin's binding affinity which was confirmed by my results. The K_d of R22E eotaxin was 20.0 nM, representing a 29.0 fold decrease in binding affinity compared to wild type eotaxin. The K_d of K44A was 4.7 nM, indicating a 7.8-fold decrease in binding affinity. Eotaxin Arg16 (Arg18 in MIP-1 β) is located near D141 and D143 of vCCI. The affinity decrease of R16A eotaxin is about 11-fold,

Table 2.1. Binding affinity constants (Kd) of eotaxin variants

Eotaxin variant	1st round K_d (nM)	2nd round K_d (nM)	3st round K_d (nM)	K_d (nM)	Relative binding affinity ($K_{dmutant}/K_{dwt}$)
WT eot	0.48	0.99	0.6	0.69 +/- 0.27	1.0
F11A eot	5.78	7.99	4.94	6.24 +/- 1.57	9.0
R16A eot	7.34	6.4	9.07	7.60 +/- 1.35	11.0
R22E eot	19.45	16.79	23.79	20.01 +/- 3.53	29.0
K44A eot	4.61	5.24	4.29	4.71 +/- 0.48	7.8
K47A eot	0.89	0.81	1.78	1.16 +/- 0.54	1.7
R16AR22E eot	No binding	No binding	No binding	No binding	no binding
R22AR44A eot	46.23	64.9	51.13	54.09 +/- 9.68	78.4
R22EK44A eot	No binding	No binding	No binding	No binding	no binding

Comparison of wild type and mutant eotaxin in a competition binding experiment

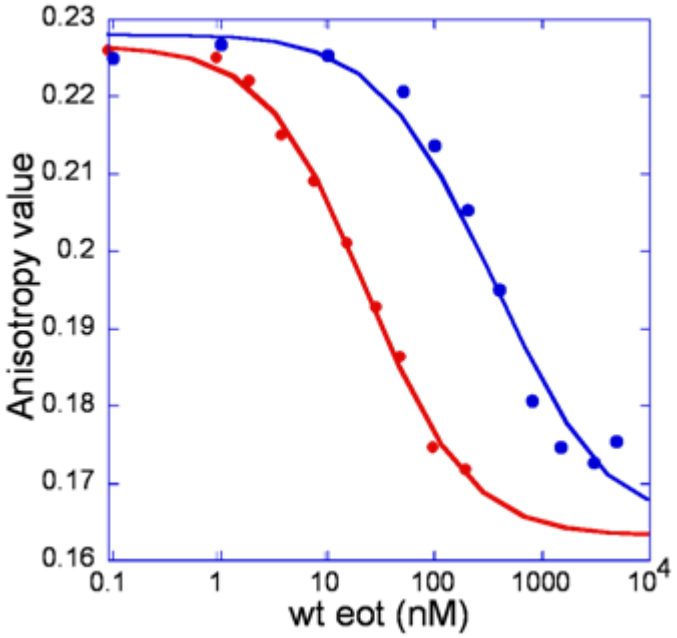

Figure 2.9. Competition binding curve for eotaxin mutants against eot-fluo. Anisotropy signal from eotaxin-fluo bound to vCCI decreases in the presence of eotaxin variant competitor. WT eotaxin competition curve is shown as red, R22E eotaxin competition curve is shown as blue. Red is wild type eotaxin competing with eot-fluo to bind vCCI; Blue is eotaxin mutant competing with eot-fluo.

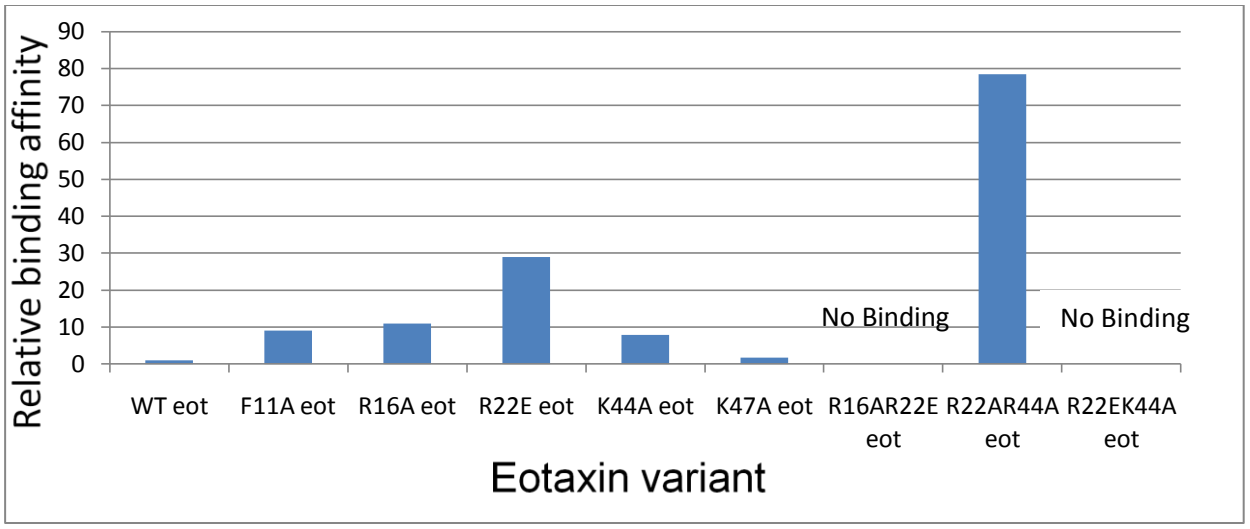

Figure 2.10. Relative binding difference between wild type eotaxin and mutants based on Kd values. Using wild type eotaxin as reference, the decrease of binding affinity of F11A eot, R16A eot, R22A eot, R44A eot, K47A eot was individually 8 fold, 10 fold, 28 fold, 6.8 fold, 0.7 fold. The binding affinity of double mutants, R16A/R22E eot, R22E/K44A eot , R22A/K44A eot , was abolished.

Table 2.2. Half maximal inhibitory concentration values (IC50) of eotaxin variants

Eotaxin variant	1st round IC_{50} (nM)	2nd round IC_{50} (nM)	3rd round IC_{50} (nM)	IC_{50} (nM)	Relative binding affinity ($IC_{50mutant}/IC_{50wt}$)
WT eot	10.91	22.75	16.51	16.72 +/- 5.92	1.0
F11A eot	112.7	136.2	95.73	114.88 +/- 20.32	6.9
R16A eot	137.2	127.3	164.45	142.98 +/- 19.24	8.6
R22E eot	375.5	315.3	416.13	368.98 +/- 50.73	22.1
K44A eot	98.2	107.2	89.92	98.44 +/- 8.64	5.9
K47A eot	24.5	21.8	38.6	28.3 +/- 9.02	1.7
R16AR22E eot	No binding	No binding	No binding	No binding	No binding
R22AR44A eot	852.4	987	813.36	884.25 +/- 91.10	52.9
R22EK44A eot	No binding	No binding	No binding	No binding	No binding

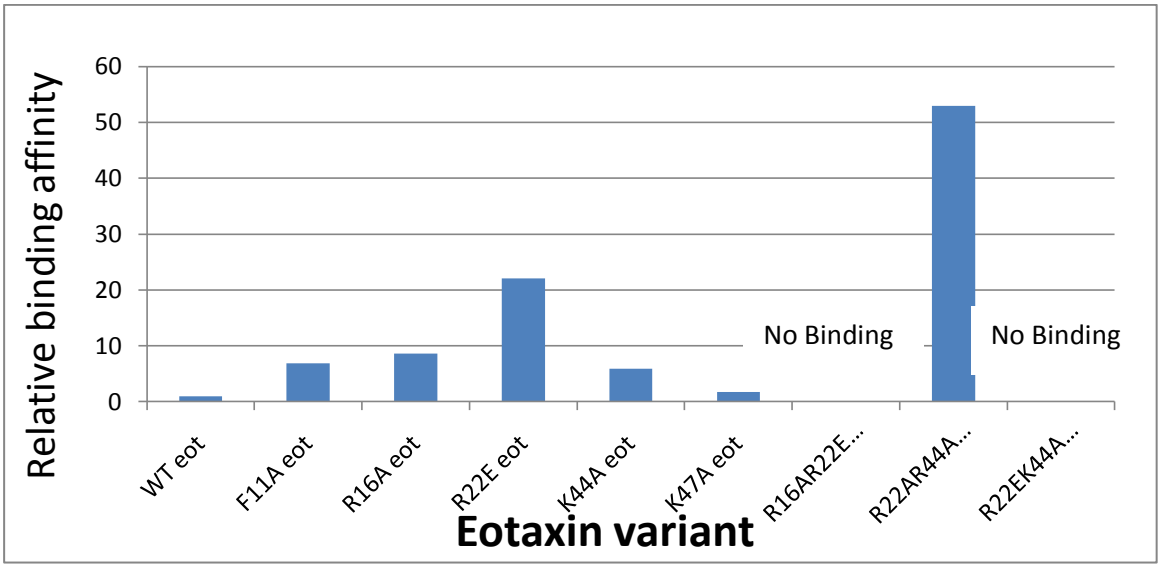

Figure 2.11. Relative binding difference between wild type eotaxin and mutants based on IC_{50} values. Using wild type eotaxin as reference, the decrease of binding affinity of F11A eot, R16A eot, R22A eot, R44A eot, K47A eot was individually 5.9 fold, 7.6 fold, 21.1 fold, 4.9 fold, 0.7 fold. The binding affinity of double mutants, R16A/R22E eot, R22E/K44A eot , R22A/K44A eot , was abolished.

representing a decent contribution to the binding. Intriguingly, all three double mutants R16A/R22E, R22E/K44A, R22A/K44A nearly abolished binding affinity to vCCI, indicating positive cooperation between residues Arg16 and Arg22. However, the abolishment of binding vCCI of R22E/K44A eotaxin and R22A/K44A eotaxin is probably because their proteins were not fold very well. Phe11 of eotaxin is located within the binding distance to the hydrophobic pocket (F217, F215, F195) of vCCI. The affinity decrease of F11A eotaxin was 9-fold, indicating Phe11 (Tyr13 in MCP-1) has moderate influence on interacting with vCCI, which agrees with the MCP-1 finding that Tyr13 has an obvious impact on binding vCCI. K47A eotaxin did not show obvious change of vCCI-binding affinity indicating Lys47 is not involved in binding even if it is located near the acidic loop.

Chapter 3

Investigation of the Essential Binding Residues of vCCI Through Mutagenesis and Fluorescence Anisotropy

3.1 Introduction

After the first structure of vCCI from cowpox virus was solved in 1999 (34), many investigations have been done on its effectiveness of anti-CC chemokine-related inflammation function (27, 28). However, there is little structural information about the interaction mechanism of specifically binding a variety of members in CC chemokine family except the discovery which showed the potential binding domains done by Zhang et al. (33). So to find those binding determinants of vCCI is the focus of this project. Analyzing the sequence alignments of those vCCI from different virus strains reveals that vCCIs share high sequence identity (more than 80%), indicating conserved characteristics in structure and function (figure 3.1). The structure of cowpox virus vCCI solved by crystallography shows a unique β-sandwich conformation with no topological resemblance to any mammalian proteins (34). In this molecule, there are two short α-helices, several loops and two parallel β-sheets. β-sheet I is composed of seven antiparallel β-strands, and its access to the solvent is blocked by two extended loops; β-sheet II is accessible to solvent, and a hydrophobic patch formed by highly conserved vCCI residues and several negatively-charged sites on the surface of β-sheet II were

Figure 3.1. Sequence alignment of three members of the orthopox vCCI family showing high homology. Also included is another virus protein VACV A41 which shares low homology with vCCI proteins.

RPV: rabbit poxvirus; CPV: cowpox virus; MPV: monkeypox virus. Conserved residues are highlighted in blue. Flexible loop between β2 and β3 is in red.

VACV: vaccinia virus.

predicted to bind to the positively charged CC chemokines. In particular it was pointed out that the area around D141 and E143 and the acidic β2-β4 loop were likely to be involved in binding CC chemokines (33). As a contrast, the protein VACV A41 from vaccinia virus lacking the acidic loop shows much weaker affinity to bind to CC chemokines than vCCIs even though it has similar conformation as vCCI and also has a conserved hydrophobic patch on sheet II (40). In this chapter, we present experiments in which we have mutated key residues in vCCI to determine their importance in binding CC chemokines.

3.2 Materials and methods

Cloning of recombinant vCCI. The genes of vCCI variants Asp141Lys, Asp 141Ala, Glu143Ala, and Glu143Phe were made by Dr. Li Zhang, a former Ph.D. student, and the vector used to incorporate the genes was pPIC ZαA vector (Invitrogen, Carlsbad, CA). The double mutant Asp 141Ala/Glu143Ala was made with the Quikchange site-directed mutagenesis procedure (Stratagene, La Jolla, CA). A triple mutant Asp59Ala/Glu61Ala/Asp63A vCCI was made through a two-part overlapping PCR method. The primers for the front part of the triple mutant vCCI were forward primer, "GAGAGGCTGAAGCTGAATTCCATCATCATCA-CCACCACTTGG" which also contains EcoRI restriction site, and reverse primer "GAGTCCGAGTCAGATCCAGCT-CCCGCGGTGGCTTCAGAAGATGATTCC". The primers for the latter part were forward primer "GGAATCATCTTCTGAAGCCACCGCGGG AGCTGGATCTGACT-CGGACTC" and reverse primer "GCGCTGGCGGCCGCTCAGACACACGCTTTGA-GTTTTGTTGAATCGAT" which also contains NotI restriction site. When both parts of

target gene were produced through a PCR reaction, they were purified and mixed together along with appropriate primers. After another set of a PCR reaction and DNA purification, the full length gene of mutant Asp59Ala/Glu61Ala/Asp63Al vCCI was acquired. Among these vCCI variant genes, double mutant Asp 141Ala/Glu143Ala and triple mutant Asp59Ala/Glu61Ala/- Asp63Ala vCCI were transformed into *Pichia pastoris* strain SMD 1168H with the electroporation method following the instruction of the manufacturer's manual (EasySelect Pichia Expression kit, Invitrogen, Carlsbad, CA). Table 3.1 list the mutants made for this project.

Protein expression of recombinant eotaxin, vCCI. Plasmid of wild type eotaxin in vector pET 28a was transformed into BL21 (DE3) *E.coli* cells for protein production, the protein was expressed in LB medium (or ^{15}N minimal medium to make ^{15}N-labeled protein) with 50 mg/l kanamycin, then purified through the same protocol described in Chapter II. The proteins of vCCI variants Asp141Lys, Asp 141Ala, and Glu143Phe were made by Li Zhang using *Pichia pastoris*.

NMR Spectroscopy. Two-dimentional NMR spectra data were collected to test if the proteins are well folded; to verify the site-directed mutation of the target residue was succesful; to make sure there is binding interaction between eotaxin and vCCI. Spectra were recorded at 37 ˚C on Bruker 600 NMR spectrometer. NMR data were processed using NMRPipe (35). Methyl resonance of DSS (4,4-dimethyl-4-silapentane-1-sulfonic acid) was used as reference to calculate the chemical shifts of proton and nitrogen (41).

Table 3.1. Proteins and/or plasmids of mutants used or made made in this project

vCCI variant	Sequenced plasmid	Protein expressed
D141A	Ж	Ж
D141K	Ж	Ж
E143F	Ж	Ж
D141A/E143A	+	-
Asp59Ala/Glu61Ala/Asp63Ala	+	-

+ represents plasmid was sequenced ; - indicates plasmid was not sequenced

Ж means it was made by Li Zhang

3.3 Results

To test the binding determinants of vCCI, the first step was to demonstrate that vCCI binds to eotaxin, which was shown by comparing the ^{15}N heteronuclear single quantum correlation (HSQC) spectrum of the unbound vCCI and bound vCCI in complex with unlabeled eotaxin (Figure 3.2). Every peak of the HSQC spectrum corresponds to one N-H group of the amino acid of the protein. Addition of unlabelled eotaxin into ^{15}N-labeled vCCI caused noticeable changes of some peaks in the HSQC spectrum, indicating interaction between these two proteins. To get the spectrum exclusively from the bound vCCI, more than one equivalent of eotaxin was added in ^{15}N-labeled vCCI to remove resonances from unbound vCCI. Drastic spectral changes were detected in bound vCCI (eotaxin :vCCI), indicating there were interactions between eotaxin and vCCI.

To determine whether particular amino acids are important in binding vCCI, several mutants of vCCI were prepared (several of the results are shown in table 3.2). Before the conclusion was made that it's the residue replacement, not the global structure change of the vCCI mutants that caused any change in binding affinity, vCCI variants were checked by NMR to make sure their structures were similar as the wild type vCCI. The ^{15}N HSQC spectra of the vCCI mutants were collected and compared with type vCCI, as shown in Figure 3.3. (In this project, the HSQC spectra of D141A vCCI and E143F were not acquired due to the low concentration of protein obtained). The HSQC spectrum of D141K vCCI shows a similar pattern of peaks as that of wt vCCI (Figure 3.3).

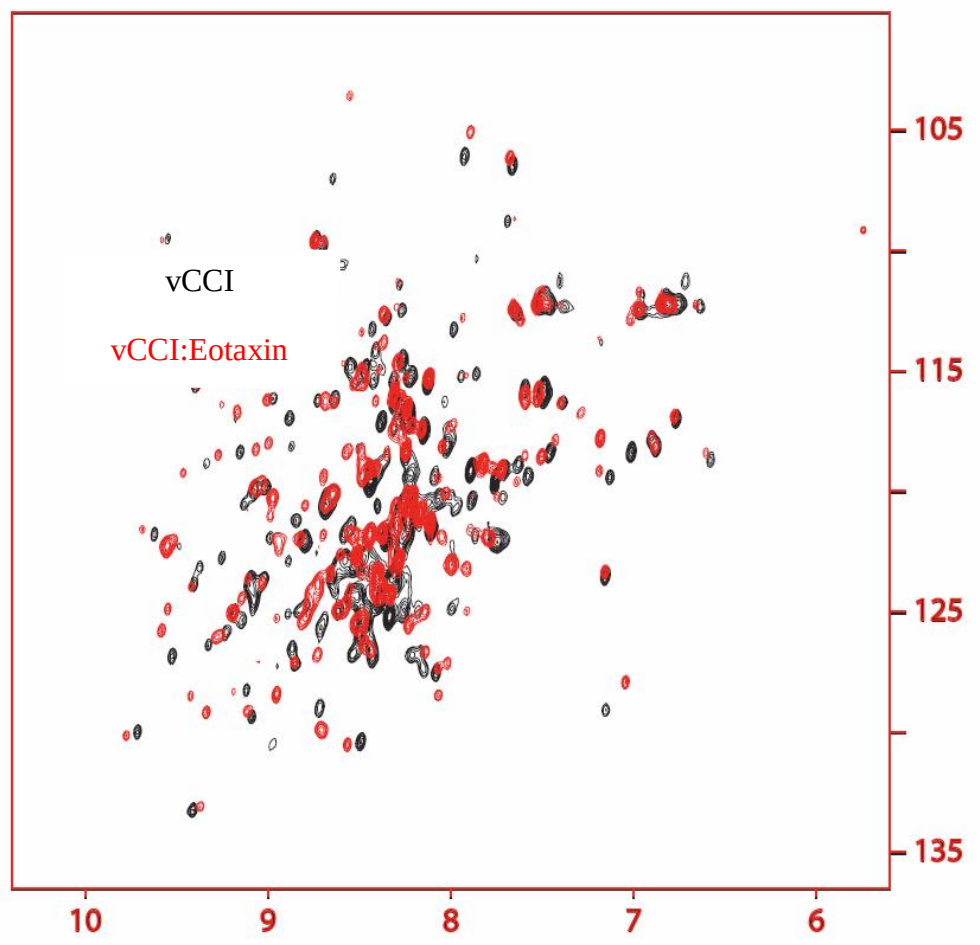

Figure 3.2. Overlay of ^{15}N HSQC of unbound vCCI (black) and complex vCCI:eotaxin (red). Eotaxin shows no peaks since it is not labeled with ^{15}N. pH:7.0; protein concentration was 1.0 mM.

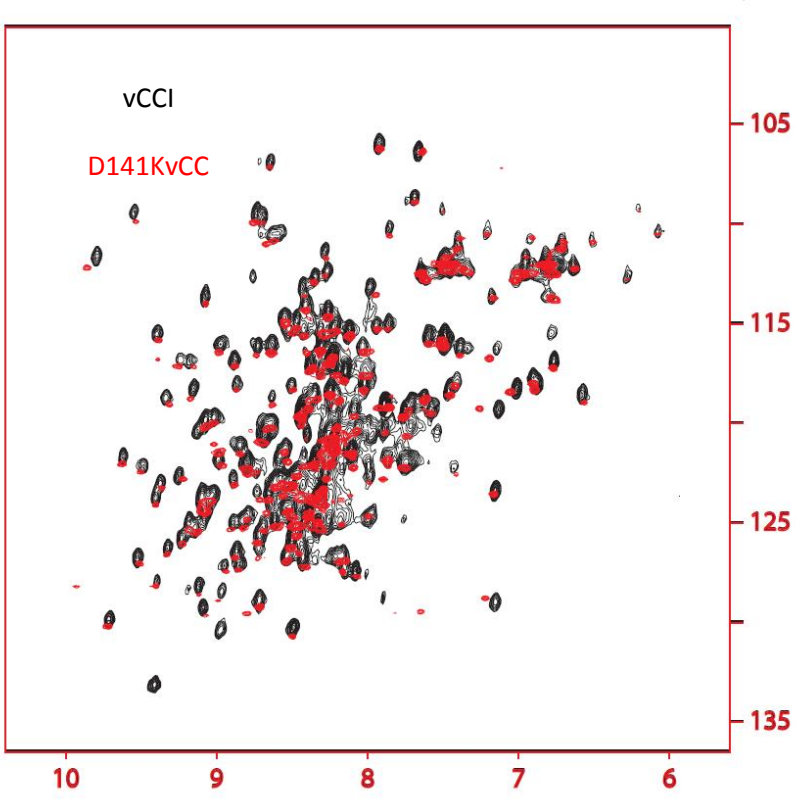

Figure 3.3. Overlay of ^{15}N HSQC of wild type vCCI (black) and D141K vCCI (red). pH:7.0; temperature: 37 °C; protein concentration of wild type vCCI was 1.0mM, ; protein concentration of D141K vCCI was 23 µM.

As described in Chapter II, fluorescence anisotropy was used to test the binding affinities between vCCI variants and eotaxin. Free eotaxin-fluor (8.6 kD) is a small molecule which rotates quickly and causes obvious depolarization shown as a small anisotropy value. However, the eotaxin-fluor:vCCI complex (35 kD) is much bigger, so it rotates slowly and causes less depolarization resulting in a bigger anisotropy value. In the titration experiments, the concentration of eotaxin-fluo was chosen as 8 nM. The anisotropy value of free eotaxin-fluo was ~ 0.165. With the gradual addition of vCCI, the anisotropy value was increased untill all eotaxin-fluo was fully bound. The total change in anisotropy is around 0.055 between free eotaxin-fluo and bound eotaxin-fluo. Based on the published structural information of MIP-1β:vCCI (shown in Figure 1.4), vCCI interacts with MIP-1β through residues from across β sheet II and the loop between the β2 and β3 strands. In particular, Asp141 and Glu143 of vCCI is expected to make contact with Arg16 of eotaxin, Tyr217 is expected to make contact with Phe11 in eotaxin, the acidic flexible loop is close to Arg22 and K45 in eotaxin. It was predicted that site-directed mutations of Asp141, Glu143, Tyr217, flexible loop would show changes in binding affinity with eotaxin. In our experiments, single mutants on amino acids Asp141 and Glu143 were done. Figure 3.4 shows curves of a series of titration of vCCI variants with eotaxin-fluo solution. Table 3.2 shows the binding affinities of those vCCI variants, D141A, D141K and E143F vCCI. These mutants respectively showed a decrease of 2.1, 1.4, 1.5 fold in binding affinity, indicating that none of them had a significant change in binding affinity. However, more experiments focused on this potential binding domain,

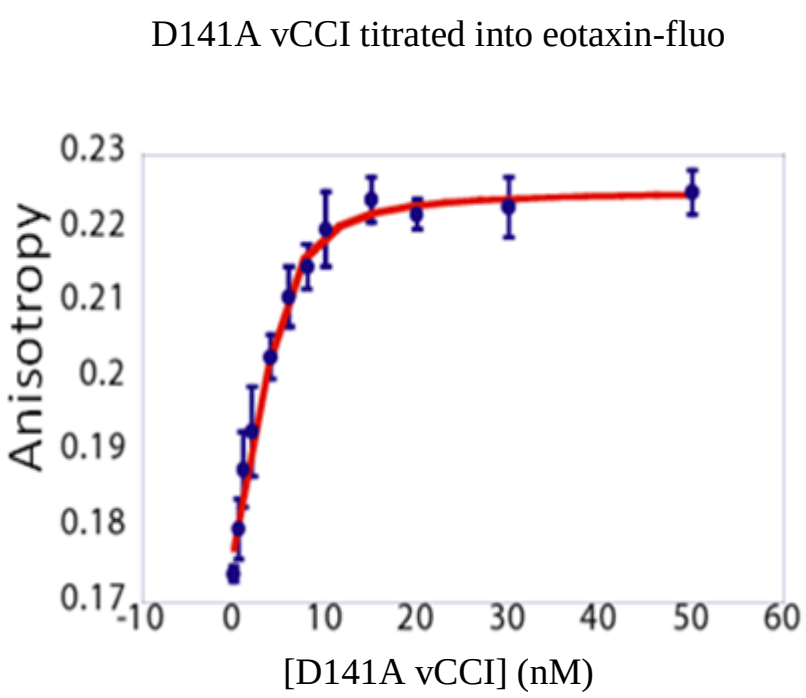

Figure 3.4. Titration of eotaxin-fluo with D141A vCCI monitored by fluorescence anisotropy.

Table 3.2. Binding affinity constants (Kd) of eotaxin variants

vCCI variant	K_d (nM)	Relative binding affinity ($K_{dmutant}/K_{dwt}$)
WT	0.89 +/- 0.32	1
D141A	2.14 +/- 0.63	2.1
D141K	1.27 +/- 0.65	1.4
E143F	1.38 +/- 0.42	1.5

such as a double mutant D141A/E143A vCCI, mutants of other nearby acidic residues (e.g. Asp73, Asp75), need to be done before any conclusion is made, regarding the importance of these residents in binding CC chemokines. As for the work on other potential binding domains, plasmids of mutants, D141A/E143A vCCI, Asp59Ala/Glu61Ala/Asp63Ala vCCI, partially-truncated flexible loop vCCI were successfully made, but proteins have not yet been produced.

Chapter 4

Making Crystals of the Complex Composed of Eotaxin and vCCI

4.1 Introduction

Given the fact that many chemokines are involved in inflammation-related diseases such as asthma, arthritis, and that vCCI can bind to a broad spectrum of CC-chemokines with high affinity, it's valuable to investigate how those CC-chemokines interact with vCCI. This could give us the insight information of how to design therapeutic agents to treat certain inflammation-related diseases. Currently there is only one publication revealing the structural features of the complex composed of a human CC chemokine (MIP-1β) and a vCCI (rabbitpox vCCI) which was done by Zhang et al. (37) using NMR. Considering the size of vCCI (26 kDa), it's challenging to completely solve the structure of the complex consisting of vCCI and a CC-chemokine by NMR since there is both spectral overlap and loss of signal caused by fast relaxation. An alternative technique to study protein structure is crystallography, whose major limitation is the availability of the crystal. In this chapter, the process of producing crystals of the complex composed of eotaxin and vCCI will be described.

4.2 Materials and methods

Protein expression of recombinant eotaxin, vCCI. Plasmid of wild type eotaxin in vector pET 28a was transformed into BL21 (DE3) *E.coli* cells for protein production, the protein was expressed in LB medium with 50 mg/l kanamycin, then purified through the

same protocol described in Chapter II. The vCCI protein was also expressed following the same protocol as described in ChapterII.

Preparing crystal screening plate to produce crystals of the complex of eotaxin:vCCI: 11.6 mg freshly produced vCCI (0.43 mmol) were freshly produced and kept in G75 pH 7.0 buffer consisting of 10 mM NaPi, 150 mM NaCl. then 5.5 mg eotaxin powder (0.62 mmol) was added into the solution. The mixture was then purified through G75 size-exclusion column to get rid of unbound eotaxin and vCCI. The fractions of the major peaks (Figure 4.1.1, fraction 3 and 4) were collected and checked by SDS-PAGE (Figure 4.1.2), then concentrated with Amicon concentrators to 300 µl with A_{280} equal to 5.6. The resulted complex was used the same day to prepare for the crystal screening plates following the protocol described in Hampton HR2-112 kit (Hampton Research, Aliso Viejo, CA).

4.3 Results

Prepared crystal screening plates were stored in 4 °C refrigerator. After about 5 months, crystals began to be observed in screening reagent #27 (buffer: 0.1 M MES monohydrate pH 6.5; salt: 0.01 M Zinc sulfate heptahydrate; Precipitant: 25% v/v polyethylene glycol monomethyl ether 550), shown in Figure 4.2. The crystals had needle-like shape, and their size was not big enough for X-ray data collection. Further work was done to reproduce the crystals in optimized screening condition derived from screening reagent #27. New crystals shown in Figure 4.3 (Photos were taken under regular optical microscope, not stereoscopic microscope) were produced in optimized

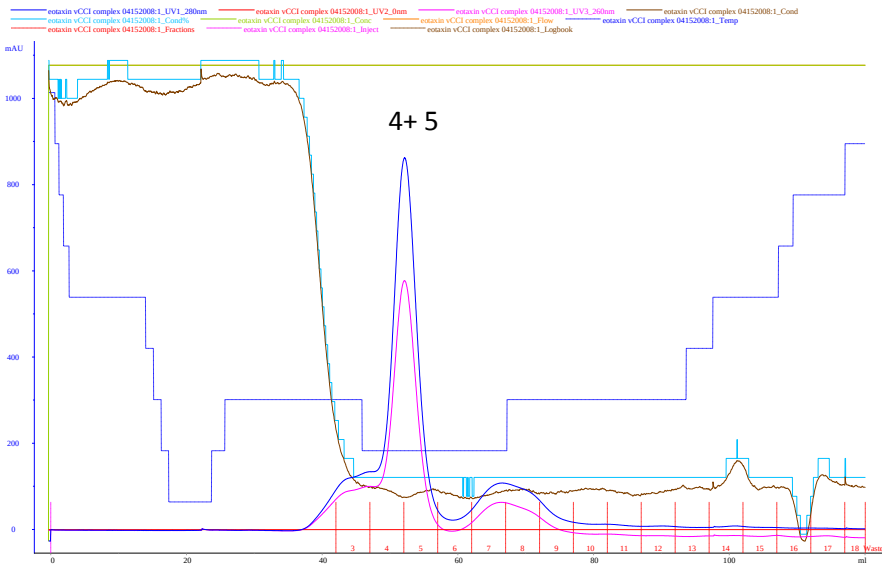

Figure 4.1.1. Elution spectrum of the complex of eotaxin:vCCI using G75 size exclusion column. Protein concentration: eotaxin was 5.5 mg; vCCI was 11.6 mg. Elution buffer system: 10 mM NaPi, 150 mM NaCl.

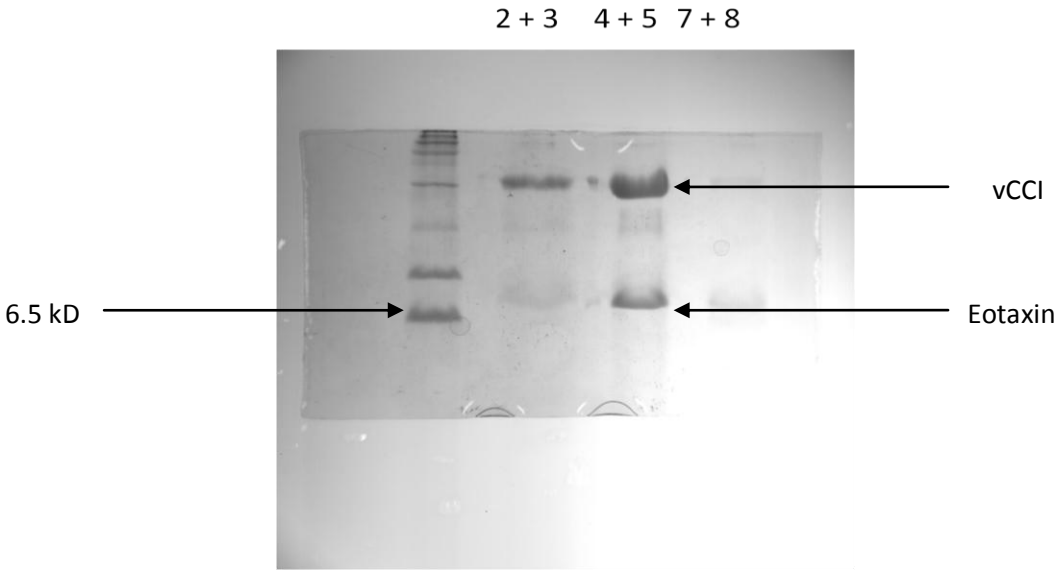

Figure 4.1.2. Commassie blue staining image of the SDS-PAGE of the fractions eluted from G75 size column

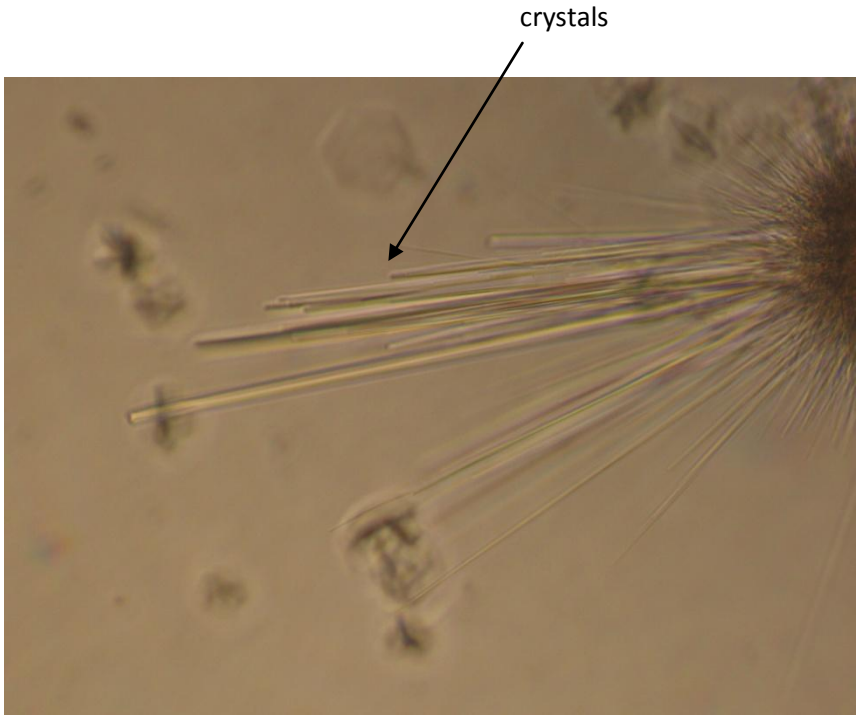

Figure 4.3. Crystals with needle-like shape were observed by optical microscope with 100 fold amplification. Screening reagent: 0.1 M MES monohydrate pH 6.5; 0.01 M Zinc sulfate heptahydrate; 25% v/v polyethylene glycol monomethyl ether 550. Temperature: 4 °C.

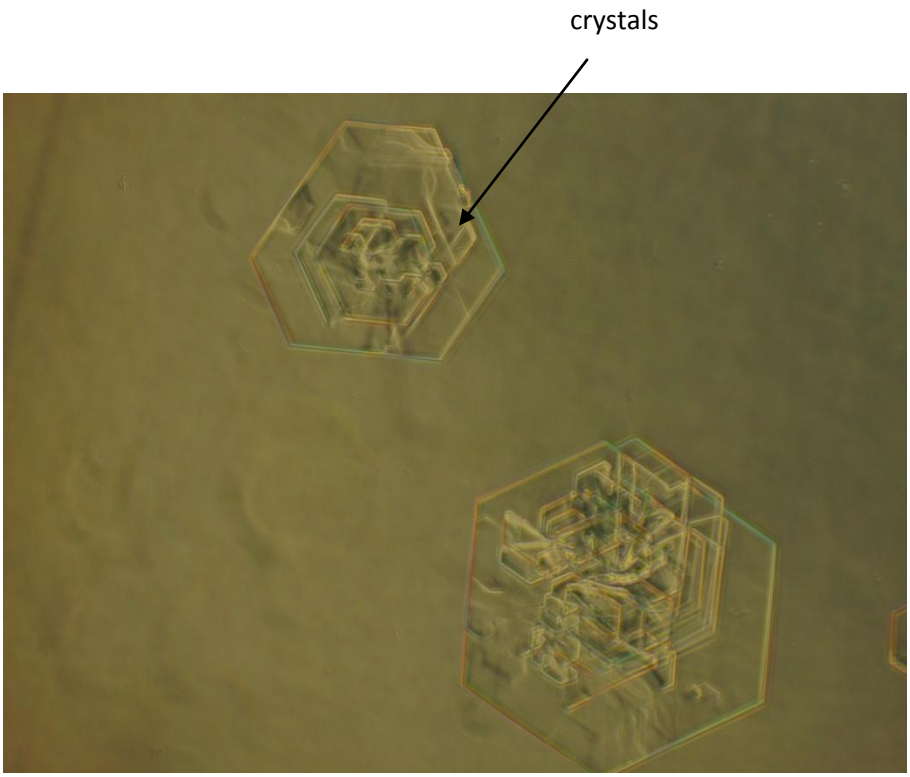

Figure 4.4. Crystals observed by optical microscope with 100 fold amplification. Screening reagent: 0.01 M Zinc sulfate heptahydrate, 0.1 M MES monohydrate pH6.5 and 30% v/v polyethylene glycol monomethyl ether 550. Temperature: 25 °C

screening reagent stored in room temperature, which consisted of 0.01 M Zinc sulfate heptahydrate, 0.1 M MES monohydrate pH6.5 and 30% v/v polyethylene glycol monomethyl ether 550. Under stereoscopic microscope (photos were unavailable), these crystals had a diamond shape with some degree of distortion. The size of these crystals had an average diameter of about 0.1 mm. Experiments to check the composition of the crystals have not yet been done.

Chapter 5

Summary and Conclusion

Through site-directed mutagenesis and anisotropy techniques, we investigated several structural determinants of eotaxin binding to vCCI. Among those residues that are important in binding vCCI, Phe11 of eotaxin is located in the N-loop which is also the binding domain that is involved in homodimerization and interacting with its receptors. Arg16, Arg22 and Lys45 are located in the domains that participate in receptor-binding and/or GAG binding. This eotaxin-binding pattern of vCCI shows the general strategy to interfere with the immune system: The chemotaxis of immune cells is inhibited when the GAG binding and dimerization of CC chemokines are occluded by the vCCI which leads to the disruption of the chemokine gradient. Through competing with the CC chemokine receptors to bind the CC chemokine, the inflammation response of those immune cells is decreased. This result matches the findings of other publications about CC chemokine binding vCCI (e.g. MCP-1) even though they used different binding assays such as Surface Plasmon Resonance and ELISA. The result also verifies the conserved pattern shared by CC chemokines that tightly bind vCCI: Using MCP-1 as a reference for amino acid numbering, position 13 is usually a hydrophobic residue, position 18 is positively charged. There must be at least one positively charged amino acid in the 24/45 position. If they are lacking a positively charged residue in both 24 and 45 position, then position 46 needs to be positively charged, likely to compensate. In contrast, for those chemokines that show low or no affinity to vCCI, such as MDC, this pattern is not observed.

The technique of anisotropy used in this project is relatively simple and operation-friendly with high sensitivity. The binding reaction is in solution which is easy to prepare and to collect data. The K_d value of wild type eotaxin binding vCCI was found to be at the nanomolar level which matches the results of other publications.

Some single-site mutants of vCCI have been investigated, and showed similar binding performance as the wild type vCCI. Given the large size of vCCI with quite a few of potential binding domains, cooperation of several residues is probably involed for vCCI to bind CC chemokines so that a single change does not have much effect. More mutants of vCCI need to be investigated in order to establish a thorough understanding of how vCCI interacts with eotaxin.

Starting from the results of vCCI binding to eotaxin, more complex, such as vCCI:MIP-1β, vCCI:MCP-1, can be analyzed with the established techniques: NMR, anisotropy and crystallography. This knowledge can help us design therapeutic reagents to treat a variety of inflammatory diseases.

Supplemental material

1. Curve fitting formulas for competition binding. The process to establish the curve fitting formula for data of competition binding was described by Viete et al. in reference 42.

Competition binding formula for curve-fitting

$a_1 = ((K_L U_T + K_U L_T - (K_L - K_U)(R_T + L_T + K_L))/(K_L - K_U))$

$a_2 = ((L_T(R_T(K_L - K_U) - K_U L_T - K_L U_T - R_T K_U - K_L K_U))/(K_L - K_U))$

$a_3 = ((R_T L_T^2 K_U)/(K_L - K_U))$

$\Theta = (\arccos(R/Q^{3/2}))$

$Q = ((a_1^2 - 3a_2)/9)$

$R = ((2a_1^3 - 9a_1a_2 + 27a_3)/54)$

(1) $Ku = K_L$

$[RL] = -b +/- (b^2 - 4ac)^{1/2}/2a$

$= (-a_2 - (a_2^2 - 4a_1a_3)^{1/2})/(2a_1)$

$= (-(L_T(R_T(K_L - K_U) - K_U L_T - K_L U_T - R_T K_U - K_L K_U)) - ((L_T(R_T(K_L - K_U) - K_U L_T - K_L U_T - R_T K_U - K_L K_U))^2 - 4(K_L U_T + K_U L_T - (K_L - K_U)(R_T + L_T + K_L))*(R_T L_T^2 K_U))^{1/2})/(2(K_L U_T + K_U L_T - (K_L - K_U)(R_T + L_T + K_L)))$

(2) $Ku > K_L$

$[RL] = -2*(Q)^{1/2} * \cos(\Theta/3) - (a1/3)$

$= -2*((a_1^2 - 3a_2)/9)^{1/2} * \cos(\text{invcos}(R/Q^{3/2})/3) - (a1/3)$

$= -2*((a_1^2 - 3a_2)/9)^{1/2} * \cos(\text{invcos}(((2a_1^3 - 9a_1a_2 + 27a_3)/54)/((a_1^2 - 3a_2)/9)^{3/2})/3) - (a1/3)$

$= 2*((((K_LU_T + K_UL_T – (K_L – K_U)(R_T + L_T + K_L))/(K_L – K_U))^2-3((L_T(R_T(K_L-K_U)- K_UL_T – K_LU_T – R_TK_U – K_LK_U))/(K_L – K_U)))/9)^{1/2} * cos(invcos(((2((K_LU_T + K_UL_T – (K_L – K_U)(R_T + L_T + K_L))/(K_L – K_U))^3-9((K_LU_T + K_UL_T – (K_L – K_U)(R_T + L_T + K_L))/(K_L – K_U))*((L_T(R_T(K_L-K_U)- K_UL_T – K_LU_T – R_TK_U – K_LK_U))/(K_L – K_U))+27((R_TL_T^2K_U)/(K_L – K_U)))/54)/((((K_LU_T + K_UL_T – (K_L – K_U)(R_T + L_T + K_L))/(K_L – K_U))^2-3((L_T(R_T(K_L-K_U)- K_UL_T – K_LU_T – R_TK_U – K_LK_U))/(K_L – K_U)))/9)^{3/2})/3) - (((K_LU_T + K_UL_T – (K_L – K_U)(R_T + L_T + K_L))/(K_L – K_U))/3)$

(3) $Ku<K_L$

$[RL] = -2*(Q)^{1/2} * \cos((\Theta+4\pi)/3) - (a1/3)$

$= -2/3*(a_1\text{^}2-3a_2)\text{^}0.5 * \cos((\text{invcos}(R/Q\text{^}(3/2)) + 4*3.14)/3) - (a1/3)$

$= -2/3*(a_1\text{^}2-3a_2)\text{^}0.5 * \cos((\text{invcos}((2a_1^3-9a_1a_2+27a_3)/54/(a_1\text{^}2/9-3*a_2/9)\text{^}(3/2)) + 4*3.14)/3) - (a1/3)$

$= -2/3*(((K_{L*}U_T + K_{U*}L_T – (K_L – K_U)*(R_T + L_T + K_L))/(K_L – K_U))\text{^}2-3*((L_T*(R_T*(K_L-K_U)- K_{U*}L_T – K_{L*}U_T – R_{T*}K_U – K_{L*}K_U))/(K_L – K_U)))\text{^}0.5 * \cos((\text{invcos}((2*((K_{L*}U_T + K_{U*}L_T – (K_L – K_U)*(R_T + L_T + K_L))/(K_L – K_U))\text{^}3-9*((K_{L*}U_T + K_{U*}L_T – (K_L – K_U)*(R_T + L_T + K_L))/(K_L – K_U))* ((L_{T*}(R_{T*}(K_L-K_U)- K_{U*}L_T – K_{L*}U_T – R_{T*}K_U – K_{L*}K_U))/(K_L – K_U)) +27* ((R_{T*}L_T\text{^}2*K_U)/(K_L – K_U)))/54/(((K_{L*}U_T + K_{U*}L_T – (K_L – K_U)*(R_T + L_T + K_L))/(K_L – K_U))\text{^}2/9-3* ((L_{T*}(R_{T*}(K_L-K_U)- K_{U*}L_T – K_{L*}U_T – R_{T*}K_U – K_{L*}K_U))/(K_L – K_U))/9)\text{^}(3/2)) + 4*3.14)/3) - (((K_{L*}U_T + K_{U*}L_T – (K_L – K_U)*(R_T + L_T + K_L))/(K_L – K_U))/3)$

REFERENCE

1. Charles, J.J. and Paul, T. Immunobiology - the immune system in health and disease. Garland Publishing, Inc. Fifth edition, 2001.

2. Ono, S. J., Nakamura, T., Miyazaki, D., Ohbayashi, M., Dawson, M., Toda, M. (2003) Chemokines: Roles in leukocyte development, trafficking, and effector function. *J. Allergy Clin. Immunol. 111*, 1185-99.

3. Butcher, E. C., Picker, L.J. (1996) Lymphocyte homing and homeostasis. *Science. 272(5258)*, 60-6.

4. Kunkel, E., Butcher, E. (2002) Homeostatic chemokines and the targeting of regional immunity. *Adv. Exp. Med. Biol. 512*, 65-72.

5. Walz, A., Peveri, P., Aschauer, H., and Baggiolini, M. (1987) Purification and amino acid sequencing of NAF, a novel neutrophil-activating factor produced by monocytes. *Biochem. Biophys. Res. Commun. 149*, 755—761.

6. Baggiolini, M. (2001) Chemokines in pathology and medicine. *J. Intern. Med. 250*, 91-104.

7. Lodi, P. J., Garrett, D. S., Kuszewski, J., Tsang, M. L.-S., Weatherbee, J. A., Leonard, W. J., Gronenborn, A. M., and Clore, G. M. (1994) High-resolution solution structure of the β chemokine hMIP-1β by multidimensional NMR. *Science 263*, 1762-1767.

8. Crump, M. P., Rajarathnam, K., Kim, K. S., Clark-Lewis, I., and Sykes, B. D. (1998) Solution structure of eotaxin, a chemokine that selectively recruits eosinophils in allergic inflammation. *J. Biol. Chem. 273*, 22471-22479.

9. Farzan, M., Choe, H., Vaca, L., Martin, K., Sun, Y., Desjardins, E., Ruffing, N.,Wu, L., Wyatt, R., Gerard, N., Gerard, C., and Sodroski, J. (1998) A tyrosinerich region in the N terminus of CCR5 is important for human immunodeficiency virus type 1 entry and mediates an association between gp120 and CCR5. *J.Virol 72*, 1160-4.

10. Fong, A. M., Alam, S. M., Imai, T., Haribabu, B., and Patel, D. D. (2002) CX3CR1 tyrosine sulfation enhances fractalkine-induced cell adhesion. *J. Biol. Chem. 277(22),* 19418-23.

11. Preobrazhensky, A. A., Dragan, S., Kawano, T., Gavrilin, M. A., Gulina, I. V., Chakravarty, L., and Kolattukudy, P. E. (2000) Monocyte chemotactic protein-1 receptor CCR2B is a glycoprotein that has tyrosine sulfation in a conserved extracellular N-terminal region. *J. Immunol. 165(9),* 5295-303.

12. Blanpain, C., Doranz, B. J., Bondue, A., Govaerts, C., De Leener, A., Vassart, G., Doms, R. W., Proudfoot, A., and Parmentier, M. (2003) The core domain of chemokines binds CCR5 extracellular domains while their amino terminus interacts with the transmembrane helix bundle. *J. Biol. Chem. 278*, 5179-87.

13. Fernando, H., Chin, C., Rösgen, J. and Rajarathnam, K. (2004) Dimer Dissociation Is Essential for Interleukin-8 (IL-8) Binding to CXCR1 Receptor. *Journal of Biological Chemistry, 279,* 36175-36178.

14. McCornack, M. A., Boren, D. M., and LiWang, P. J. (2004) Glycosaminoglycan disaccharide alters the dimer dissociation constant of the chemokine MIP-1 beta. *Biochemistry 43*, 10090-101.

15. Jin, H., Shen, X., Baggett, B., Kong, X., and LiWang, P. The Human CC Chemokine MIP-1β Dimer Is Not Competent to Bind to the CCR5 Receptor. (2007) *The Journal of Biological Chemistry, 282,* 27976-27983.

16. Gerard, C., and Rollins, B. J. (2001) Chemokines and disease. *Nat. Immunol. 2*, 108-115.

17. Olson, T. S., Ley, K. (2002) Chemokines and chemokine receptors in leukocyte trafficking. *Am. J. Physiol. Regul. Integr. Comp. Physiol. 283*, R7-28

18. Ogilvie, P., Bardi, G., Clark-Lewis, I., Baggiolini, M., Uguccioni, M. (2001) "Eotaxin is a natural antagonist for CCR2 and an agonist for CCR5". Blood. 97(7), 1920–1924.

19. Juremalm, M., Nilsson, G. (2005) Chemokine receptor expression by mast cells. *Chem Immunol Allergy. 87,* 130-44.

20. ROTTMAN, J. B. (1999) Key Role of Chemokines and Chemokine Receptors in Inflammation, Immunity, Neoplasia, and Infectious Disease. *Vet Pathol, 36,* 357–367.

21. Thelen, M. (2001) Dancing to the tune of chemokines. *Nat. Immunol. 2(2),* 129-34.

22. Lau, E. K., Allen, S., Hsu, A. R., and Handel, T. M. (2004) Chemokine-receptor interactions: GPCRs, glycosaminoglycans and viral chemokine binding proteins. *Adv. Protein Chem. 68,* 351-91.

23. Baggiolini, M. (2001) Chemokines in pathology and medicine. *J. Intern. Med. 250*, 91-104.

24. Nives, Z., Gurjit, K. H., Paul, S. F. and Marc,E.R. (2003) Chemokines in asthma: Cooperative interaction between chemokines and IL-13. *Journal of Allergy and Clinical Immunology.111(2),* 227-242.

25. Gaoyun, Y., Li, L., Amy, V., Eva, E., Ted, P., Jill, G.K., Patricia, R., Mani, L., et al. Therapeutic Dosing with Anti-Interleukin-13 Monoclonal Antibody Inhibits Asthma, Progression in Mice. *Journal of Pharmacology And Experimental Therapeutics. 313(1).* 8-15.

26. Seet, B. T., and McFadden, G. (2002) Viral chemokine-binding proteins. *J. Leukoc. Biol. 72,* 24-34.

27. Lalani, A. S., Graham, K., Mossman, K., Rajarathnam, K., Clark-Lewis, I., Kelvin, D., and McFadden, G. (1997) The purified myxoma virus gamma interferon receptor homolog M-T7 interacts with the heparin-binding domains of chemokines. *J. Virol. 71,* 4356-63.

28. van Berkel, V., Barrett, J., Tiffany, H. L., Fremont, D. H., Murphy, P. M., McFadden, G., Speck, S. H., and Virgin, H. I. (2000) Identification of a

gammaherpesvirus selective chemokine binding protein that inhibits chemokine action. *J. Virol. 74*, 6741-7.

29. Graham, K. A., Lalani, A. S., Macen, J. L., Ness, T. L., Barry, M., Liu, L. Y., Lucas, A., Clark-Lewis, I., Moyer, R. W., and McFadden, G. (1997) The T1/35kDa family of poxvirus-secreted proteins bind chemokines and modulate leukocyte influx into virus-infected tissues. *Virology 229*, 12-24.

30. Burns, J. M., Dairaghi, D. J., Deitz, M., Tsang, M., and Schall, T. J. (2002) Comprehensive mapping of poxvirus vCCI chemokine-binding protein. Expanded range of ligand interactions and unusual dissociation kinetics. *J. Biol. Chem. 277*, 2785-9.

31. Reading, P.C., Symons, J.A. and Smith, G.L. (2003) A soluble chemokine-binding protein from vaccinia virus reduces virus virulence and the inflammatory response to infection. *J Immunol. 170(3)*, 1435–1442.

32. Jones, J.M., Messauodi, I., Estep, R.D., Orzechowska, R. and Wong, S.W. (2008) Monkeypox virus viral chemokine inhibitor (MPV vCCI), a potent inhibitor of rhesus macrophage inflammatory protein-1. *Cytokine. 43(2)*, 220-228.

33. Lalani, A. S., Ness, T. L., Singh, J. K., Harrison, J. K., Seet, B. T., Kelvin, D. J., McFadden, G., and Moyer, R. W. (1998) Functional comparisons among 91 members of the poxvirus T1/35kDa family of soluble CC-chemokine inhibitor glycoproteins. *Virology 250*, 173-184.

34. Carfi, A., Smith, C. A., Smolak, P. J., McGrew, J., and Wiley, D. C. (1999) Structure of a soluble secreted chemokine inhibitor vCCI (p35) from cowpox virus. *Proc. Natl. Acad. Sci. U.S.A. 96*, 12379-12383.

35. Seet, B. T., Singh, R., Paavola, C., Lau, E. K., Handel, T. M., and McFadden, G. (2001) Molecular determinants for CC-chemokine recognition by a poxvirus CCchemokine inhibitor. *Proc. Natl. Acad. Sci. U.S.A. 98*, 9008-13.

36. Beck, C. G., Studer, C., Zuber, J. F., Demange, B. J., Manning, U., and Urfer, R. (2001) The viral CC chemokine-binding protein vCCI inhibits monocyte chemoattractant protein-1 activity by masking its CCR2B-binding site. *J. Biol.Chem. 276*, 43270-6.

37. Zhang, L., DeRider, M., McCornack, A.M., Jao, S., Isern, N., Ness, T., Moyer, R., LiWang, P.J. (2006) Solution structure of the complex between poxvirus-encoded CC chemokine inhibitor vCCI and human MIP-1β. *PNAS. 103(38),* 13985-13990.
K.E. van Holde, W.C. Johnson and P.S. Ho

38. Van Holde, K.E., Johnson, W.C., Ho, P.S. (1998) Principles of physical biochemistry. Prentice-Hall, Upper Saddle River, New Jersey, 519.

39. Delaglio, F., Grzesiek, S., Vuister, G. W., Hu, G., Pfeifer, J., and Bax, A. (1995) NMRPipe: A multidimensional spectral processing system based on UNIX pipes. *J. Biomol. NMR 6,* 277-293.

40. Bahar, M.W., Kenyon, J.C., Putz, M.M., Abrescia, N.G.A., Pease, J.E., Wise, E.L., Stuart, D.I., Smith, G.L., and Grimes, J.M. (2008) Structure and Function of A41, a Vaccinia Virus Chemokine Binding Protein. *PLoS Pathog. 4(1),* e5. 55-68.

41. Wishart, D. S., Bigam, C. G., Yao, J., Abildgaard, F., Dyson, H. J., Oldfield, E., Markley, J. L., and Sykes, B. D. (1995) 1H, 13C, 15N chemical shift referencing in biomolecular NMR. *J. Biomol. NMR 6,* 135-140.

42. Huff, S., Mastsuka, V.Y., McGavin, J.M., and Ingham K.C. (1994) Interaction of N-terminal fragments of fibronectin with synthetic and recombinant D motifs from its binding protein on Staphylococcus aureus studied using fluorescence anisotropy. *The Journal of Biological Chemistry. 269 (22),* 15563-15570.